



Alternative splicing controls cell lineage-specific responses to endogenous innate immune triggers within the extracellular matrix



Sean P. Giblin, Anja Schwenzer, and Kim S. Midwood

Kennedy Institute of Rheumatology, Nuffield Department of Orthopaedics, Rheumatology and Musculoskeletal Sciences, University of Oxford, Oxford, United Kingdom

Corresponding author at: Kennedy Institute of Rheumatology, Roosevelt Drive, Headington, Oxford, OX3 7FY, United Kingdom. kim.midwood@kennedy.ox.ac.uk.
<https://doi.org/10.1016/j.matbio.2020.06.003>

Abstract

The identification of barely more than 20,000 human genes was amongst the most surprising outcomes of the human genome project. Alternative splicing provides an essential means of expanding the proteome, enabling a single gene to encode multiple, distinct isoforms by selective inclusion or exclusion of exons from mature mRNA. However, mis-regulation of this process is associated with most human diseases. Here, we examine the impact of post-transcriptional processing on extracellular matrix function, focusing on the complex alternative splicing patterns of tenascin-C, a molecule that can exist in as many as 500 different isoforms. We demonstrate that the pro-inflammatory activity of this endogenous innate immune trigger is controlled by inclusion or exclusion of a novel immunomodulatory site located within domains AD2AD1, identifying this as a mechanism that prevents unnecessary inflammation in healthy tissues but enables rapid immune cell mobilization and activation upon tissue damage, and defining how this goes awry in autoimmune disease.

© 2020 The Authors. Published by Elsevier B.V. This is an open access article under the CC BY license (<http://creativecommons.org/licenses/by/4.0/>)

Introduction

Alternative splicing provides a remarkably efficient means of maximizing genomic diversity. Around 95% of all multi-exonic human genes are post-transcriptionally processed, creating >290,000 non-redundant peptide combinations, expanding proteomic output from a relatively modest genome of ~21,000 genes [1, 2]. However, altered splicing patterns are increasingly associated with pathology in cancer [3, 4], cardiovascular [5] and neurodegenerative [6, 7] diseases, and autoimmune conditions including multiple sclerosis, ulcerative colitis, scleroderma and rheumatoid arthritis (RA) [8, 9]. Here, loss of control over even relatively simple splicing events can result in strikingly distinct biological outcomes. For example, an imbalance in tissue levels of the two isoforms of the microtubule-associated protein tau is linked to neurofibrillary tangles and protein aggregation during the development of

dementia and Alzheimer's disease [10, 11], whilst the long and short variant of the scaffold protein intersectin-1 exert entirely opposing effects on glioblastoma disease progression [12]. However, far greater complexity of alternative splicing is also apparent, typified by the extracellular matrix protein tenascin-C, which can exist in as many as 511 different isoforms.

Tenascin-C comprises a modular structure, which includes 17 fibronectin type III-like repeats (FnIII). Eight of these domains are constitutively expressed (FnIII 1–8), whilst the other nine (FnIII A1, A2, A3, A4, B, AD2, AD1, C and D) can be alternatively spliced. Variation in the number and combination of these domains generates enormous diversity of form that has been best studied during embryogenesis and in cancer. Small isoforms (containing only FnIII 1–8) are restricted to areas of cell condensation and differentiation during organogenesis, whilst large variants (containing one or more alternatively

spliced FnIII repeat) are associated with regions of active tissue remodeling, cell migration and division (reviewed in [13]). Up-regulation of alternatively spliced domains is also common in cancer, showing promise in disease diagnosis and drug delivery. For example, high urine levels of FnIII B reliably detect, and predict, the recurrence of bladder cancer [14, 15], whilst tumor cell overexpression of FnIII A1 or FnIII C/D has been exploited for disease specific targeting of cytotoxic drugs linked to antibodies recognizing these domains, improving disease outcome for people with glioblastoma, lung cancer, breast cancer and Hodgkin's lymphoma (reviewed in [16, 17]). Mechanistically, alternative splicing can create tenascin-C isoforms with distinct receptor binding capabilities (for example inclusion of FnIII D in variants detected in the developing cerebellum provides an $\alpha 7\beta 1$ integrin binding site that promotes neurite outgrowth [18]), or with unique proteolytic susceptibilities (for example insertion of FnIII A3 provides an MMP cleavage site that is not present in constitutive FnIII domains [19]). However, the functional consequences of tenascin-C splicing are not completely understood.

One emerging aspect of tenascin-C biology is its role in immunity. Whilst widely expressed during development, it is found at low levels, or not at all, in most healthy adult tissues. Rapid and transient upregulation of tenascin-C following tissue damage or cellular stress serves as a danger signal, triggering innate immune responses designed to restore homeostasis, as well as shaping adaptive immune responses. Accumulation of high levels of tenascin-C is associated with chronic inflammation in a large number of diseases, although its role is notoriously context specific. For example, whilst tenascin-C deletion is deleterious during experimental dermatitis, glomerulonephritis and osteoarthritis, mice lacking tenascin-C are protected in models of Alzheimer's disease, asthma, RA and in dermal, liver and lung fibrosis (reviewed in [20, 21]). We hypothesized that alternative splicing dictates tissue/disease-specific roles for tenascin-C. However, surprisingly little is known about the expression or post-transcriptional processing of this molecule during inflammation. Here, we systematically examined the production of tenascin-C in immune and stromal cells, each well-documented sources of this protein during tissue injury [22, 23], using cellular models of acute and chronic inflammation. We discovered distinct, cell lineage-specific methods of tenascin-C biosynthesis across different cell types. Despite these differences we identified common splicing events linked to both immune cell and fibroblast activation. We demonstrated how disease-associated tenascin-C isoforms selectively drive pro-inflammatory cell behavior, via removal of FnIII AD1 and AD2, domains with immuno-regulatory capabilities.

These data reveal how control over innate inflammatory responses is exerted, using post-transcriptional processing to create immunologically inert or active variants of endogenous immune triggers.

Results

Cell lineage specific biosynthesis of tenascin-C in resting and activated primary human cells

Absolute levels of tenascin-C mRNA were quantified in a panel of stromal, myeloid and lymphocytic cells before stimulation. High basal levels were confirmed in human dermal fibroblasts (HDFs) [24] and U-87MG glioma cells [25], with 1000-fold lower levels detected in immune cells. Monocytes, macrophages and dendritic cells contained higher copy numbers than T-cells, whilst tenascin-C mRNA was not detected in neutrophils (Fig. 1A). Following cell activation with well-characterized, lineage-specific stimuli (Supplementary Table S1), tenascin-C mRNA was quantified over time relative to validated housekeeping genes (Supplementary Table S2). Unstimulated HDFs expressed constitutively high tenascin-C levels over time, which transiently increased upon IL-1 β stimulation, peaking between 4 and 48 h, returning to baseline by 5 days (Fig. 1B). Tenascin-C mRNA levels remained low over time in unstimulated immune cells, and whilst expression in monocytes, macrophages and dendritic cells was transiently induced following LPS activation, peaking in monocytes between 8 and 24 h, in macrophages and dendritic cells between 4 and 8 h (Fig. 1C-F), and in anti-CD3/CD28 activated CD4 $^{+}$ and CD8 $^{+}$ T-cells between 24 and 48 h (Fig. 1G, H), tenascin-C mRNA was not detected in activated neutrophils (Fig. 1I).

Tenascin-C protein was quantified by ELISA in HDFs, dendritic cells, CD4 $^{+}$ T-cells and neutrophils. HDFs constitutively expressed high levels of protein, with more secreted than associated with cells, but with a delay in secretion until 24 h after plating. IL-1 β activation significantly increased tenascin-C secretion with a trend towards higher cell-associated protein (Fig. 2A, B). Resting dendritic cells expressed low levels of protein over time, with cell-associated tenascin-C transiently increased upon LPS activation, peaking 8 h following stimulation and then declining, whilst levels started to accumulate in the supernatant from 8 h onwards (Fig. 2C, D). Tenascin-C protein was not detected in the supernatant or cell lysate of activated CD4 $^{+}$ T-cells or neutrophils. Confocal immunofluorescence revealed tenascin-C organized as fibrils, co-localizing with the fibronectin matrix, exclusively at the apical cell surface of HDFs, which increased following IL-1 β treatment (Fig. 2E, F). Cell-associated

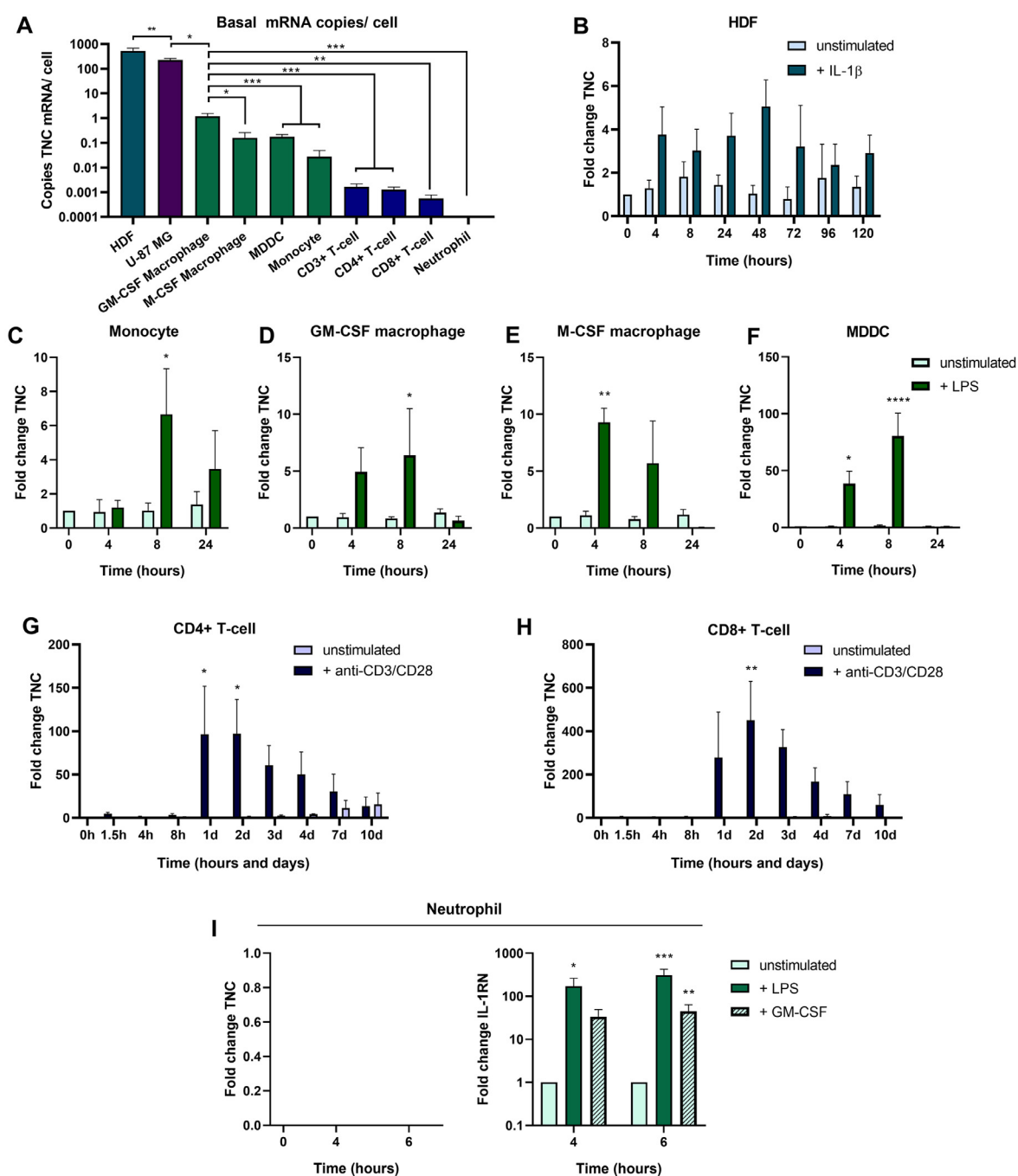


Fig. 1. Cell lineage specific quantification of tenascin-C mRNA in resting and activated primary human cells. Absolute levels of tenascin-C mRNA (*TNC*) were quantified using standard curve qPCR in HDF ($n = 6$), U-87 MG cell lines ($n = 6$), GM-CSF macrophages ($n = 8$), M-CSF macrophages ($n = 4$), monocyte-derived dendritic cells (MDDC) ($n = 8$), monocytes ($n = 5$), CD3+ T-cells ($n = 5$), CD4+ T-cells ($n = 7$), CD8+ T-cells ($n = 4$) and neutrophils ($n = 5$) before stimulation (A). Cells were then activated or left unstimulated over the time courses indicated before quantification of *TNC* using standard curve qPCR. Fold induction of *TNC* relative to levels in unstimulated cells at $t = 0$, following normalisation to control genes (*italics*) is plotted for HDFs ($n = 8$; *RPLP0*) (B), monocytes ($n = 3$; *GAPDH*) (C), GM-CSF macrophages ($n = 4$; *HPRT1*) (D), M-CSF macrophages ($n = 3$; *HPRT1*) (E), MDDCs ($n = 3$; *GNB2L1*) (F), CD4+ T-cells ($n = 6$; *YWHAZ*) (G), CD8+ T-cells ($n = 7$; *YWHAZ*) (H), and neutrophils ($n = 5$; *HPRT1*) (I). *IL1RN* mRNA was quantified in the same neutrophil samples to confirm cell activation in response to LPS and GM-CSF stimulation [86, 87]. Data are shown as mean + SEM. One-way ANOVA with Turkey's multiple comparisons was performed for HDF vs U-87 MG, and for all immune cells in A, two-way ANOVA with Sidak's multiple comparisons test was performed for B-I. Statistical significance is displayed as * $p < 0.05$, ** $p < 0.01$, *** $p < 0.001$ and **** $p < 0.0001$.

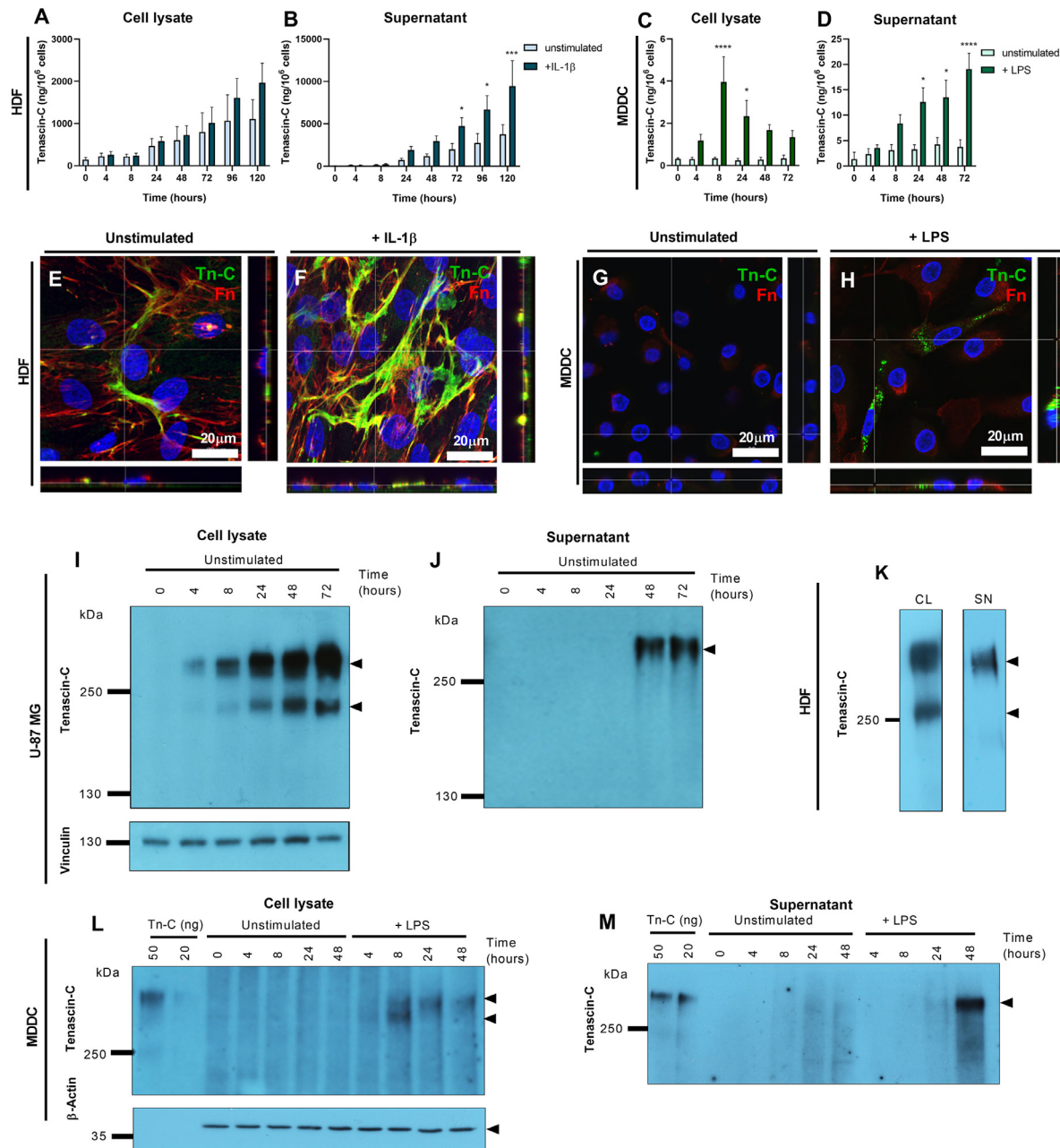


Fig. 2. Distinct tenascin-C protein expression and localization in fibroblasts and dendritic cells. Tenascin-C protein expression was quantified by ELISA in cell lysate (CL) and supernatant (SN) fractions isolated from HDFs (CL 2 μ l; SN 1 μ l; $n = 5$) (A, B) and MDDC (CL 50 μ l; SN 50 μ l; $n = 3$) (C, D) in cells that were left unstimulated, or which were stimulated for the indicated times with 10 ng/ml IL-1 β (HDF) or 10 ng/ml LPS (MDDC). Data are shown as mean \pm SEM. Two-way ANOVA with Sidak's multiple comparison tests were performed, and statistical significance is displayed as * $p < 0.05$, *** $p < 0.001$, **** $p < 0.0001$. Immunofluorescence localization of tenascin-C (green, Tn-C), fibronectin (red, FN) or cell nuclei (blue) in HDFs that were left unstimulated for 48 h (E), or which were stimulated with 10 ng/ml IL-1 β for 48 h (F), and in MDDC that were left unstimulated for 8 h (G) or stimulated for 100 ng/ml LPS for 8 h (H). Images show a representative 120x objective view from 3 independent experiments, and the corresponding z-stack cross-sections. Scale bar = 20 μ m. Tenascin-C protein was resolved by SDS-PAGE of CL and SN isolated from glioma (20 μ l) (I, J), HDFs (20 μ l) (K) and MDDC (100 μ l) (L, M). MDDC samples were run alongside samples of 20 or 50 ng of purified tenascin-C (Tn-C). Gels were Western blotted, and blots probed with antibodies against tenascin-C, before stripping and re-probing cell lysate blots with antibodies against vinculin or actin. Images are representative of 5 independent experiments.

tenascin-C was not detected in unstimulated dendritic cells, whilst LPS activation resulted in the accumulation of dense intracellular tenascin-C foci, distinct from fibronectin staining, and absent from the cell surface (Fig. 2G, H). Western blotting revealed that both HDFs and glioma expressed two cell-associated tenascin-C variants (~300 kDa and ~250 kDa), of which the larger was more abundant. Only the larger variant was detected in the supernatant (Fig. 2I-K), and this pattern did not change upon IL-1 β stimulation of HDFs (data not shown). Little tenascin-C was detected in the cell lysate or supernatant of unstimulated dendritic cells. However, LPS treatment induced two cell-associated variants (~300 kDa and ~280 kDa); the smaller band was most abundant at 8 h, whilst the larger band predominated at later time points. LPS activation induced secretion of a single large band (~300 kDa) at 24–48 h (Fig. 2L, M).

Together these data demonstrate quantitative differences in basal tenascin-C expression in distinct cell lineages, and different kinetics of tenascin-C induction upon activation with inflammatory stimuli. Stromal and immune cells also exhibited a unique distribution of tenascin-C protein; with assembly into the fibrillar, cell-associated matrix predominating in fibroblasts, compared to rapid trafficking through the cell before secretion of soluble tenascin-C in dendritic cells.

Post-transcriptional processing of tenascin-C is defined by cell activation or disease status

To investigate whether alternative splicing of tenascin-C contributes to the different tenascin-C variants observed in different cells, we used a method developed to quantify the abundance of individual alternatively spliced FnIII mRNA using standard curve qPCR [26]. In unstimulated dendritic cells, low levels of all 9 alternatively spliced FnIII were detected at comparable abundance to total tenascin-C, which was assessed by quantification of the constitutively expressed FnIII 7–8 domains. Following LPS activation, FnIII 7–8 and all alternatively spliced FnIII were significantly upregulated with the exception of FnIII AD2 and AD1; mRNA levels of these 2 domains did not change and were detected at lower levels compared to all other FnIII domains (Fig. 3A, B, Supplementary figure S1A). This pattern was also observed in LPS-activated macrophages (Supplementary Figure S1B-C). In contrast, in HDFs FnIII 7–8 was detected at higher levels than all of the alternatively spliced domains, of which FnIII B and D were the most abundant, and AD2 and AD1 the least abundant present at significantly lower levels than FnIII B and D. IL-1 β stimulation caused a proportionate increase in FnIII 7–8 and all the alternatively spliced FnIII mRNAs, such that total *TNC* mRNA levels increased but the overall splicing pattern did not change (Fig. 3C, D,

Supplementary figure S1D). Glioma cell lines exhibited a similar tenascin-C domain content to that in HDFs (Fig. 3E). To determine whether the tenascin-C splicing pattern maintained in resting and activated HDFs is universally conserved amongst fibroblasts we examined synovial fibroblasts isolated from people with healthy joints (NSF), osteoarthritis (OA-SF) or rheumatoid arthritis (RA-SF). HDFs expressed higher tenascin-C mRNA and protein than all synovial fibroblasts, with RA-SFs expressing more than OA-SFs and NSFs (Supplementary figure S1E-F). In both NSF and RA-SF, tenascin-C was predominantly fibrillar, colocalizing with fibronectin at the surface of the cell, with higher levels in the RA-SF matrix, whilst OA-SFs exhibited patchy staining of tenascin-C on the cell surface, with no visible fibrils, nor colocalization with fibronectin (Supplementary figure S1G). In both NSF and OA-SF all FnIII domains were expressed at levels comparable to FnIII 7–8, except for FnIII A1, which was undetectable. However, RA-SFs exhibited a splicing pattern that mirrored that in HDF and glioma; FnIII 7–8 was the most abundant domain, with higher levels of FnIII B and D, and lower levels of FnIII AD2 and AD1 (Fig. 3F-H).

Together these data indicate that non-activated immune cells express low basal levels of a large tenascin-C isoform containing all alternatively spliced FnIII, and that LPS activation induces the synthesis of a smaller isoform lacking FnIII AD2-AD1. These data also show that synovial and dermal fibroblasts do not process tenascin-C in the same way, and that whilst NSF and OA-SF express low levels of a large tenascin-C isoform lacking only FnIII A1, RA-SF, like HDFs and glioma cells express isoforms containing proportionately higher levels of FnIII B and D, and lower levels of AD2-AD1.

Does the alternatively spliced cassette BAD2AD1CD impact cell behaviour during inflammation?

Common to both stromal and immune cells was variation in alternative splicing of tenascin-C within the BAD2AD1CD domains. Activated myeloid cells made isoforms lacking AD2AD1, creating smaller variants in which FnIII B, C and D are likely to be expressed contiguously. This pattern was also observed in synovial fibroblasts where NSF and OA-SF expressed AD2AD1 at comparable levels to other FnIII, but RA-SF isoforms contained lower levels of AD2AD1 (Fig. 4A). These data prompted us to hypothesize that domains AD2AD1 may exert a regulatory role during inflammation. Recombinant proteins were expressed comprising domains AD2AD1, to assess any direct role of these domains on cell function; and domains BCD and BAD2AD1CD, to determine whether removal of AD2AD1 affects cell response to neighboring FnIII

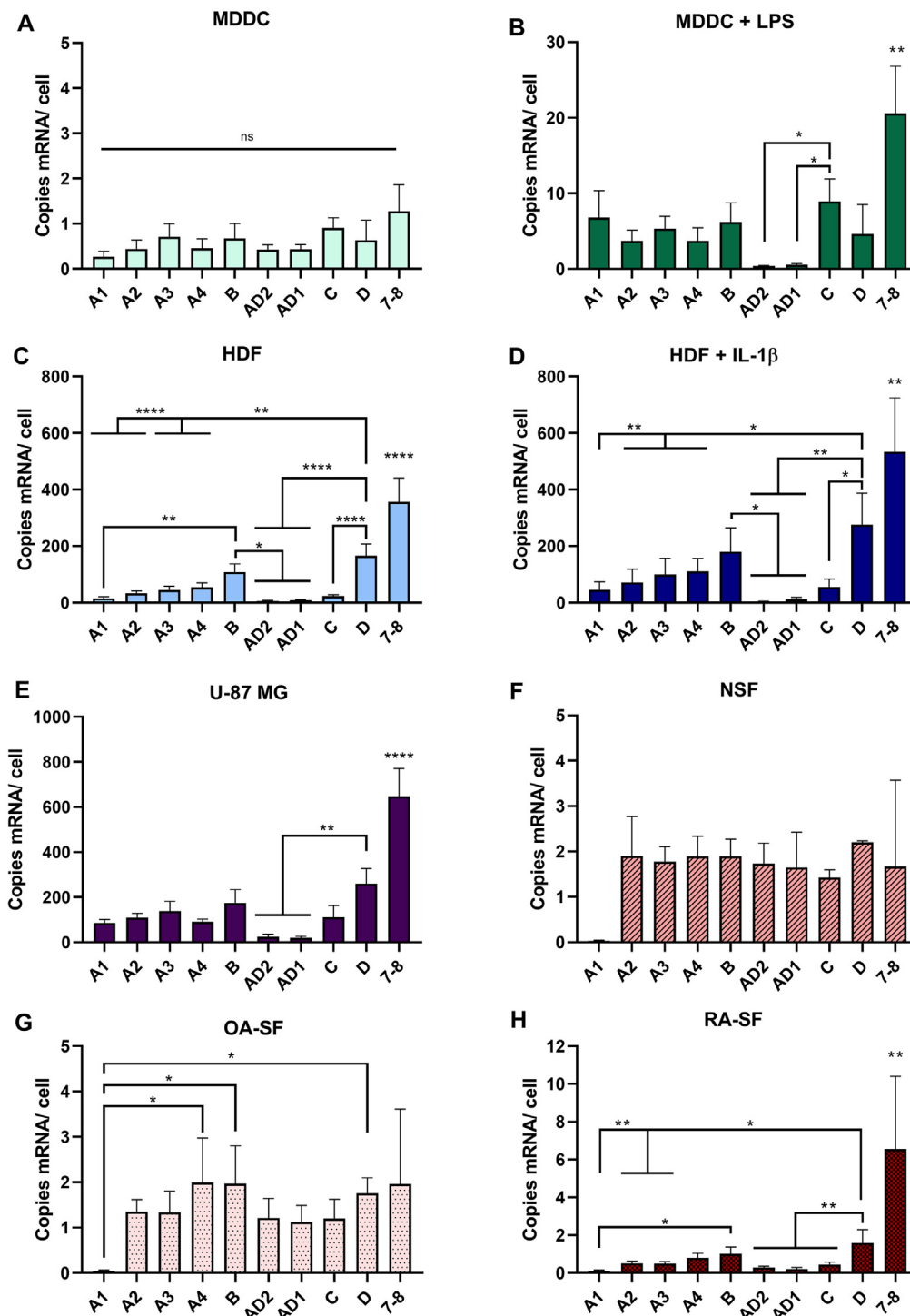


Fig. 3. Alternative splicing of tenascin-C is regulated by cell activation and disease status. The abundance of mRNA corresponding to *TNC* FnIII domains A1, A2, A3, A4, B, AD2, AD1, C and D was quantified by standard curve qPCR in MDDC that were left unstimulated ($n = 6$)(A), or were stimulated with 10 ng/ml LPS ($n = 4$)(B), HDFs that were left unstimulated ($n = 6$)(C) or were stimulated with 10 ng/ml IL-1 β ($n = 3$)(D), and in U-87 MG glioma cell lines ($n = 10$)(E), NSF ($n = 2$)(F), OA-SF ($n = 3$)(G) and RA-SF ($n = 4$)(H) that were cultured for 48 h without stimulation. The abundance of the constitutively expressed domains FnIII 7-8 was quantified in each cell type in parallel. Data are shown as mean + STDEV for $n = 2$, and as mean + SEM for $n \geq 3$. One-way ANOVA with Dunnett's multiple comparison tests were performed for FnIII 7-8 vs FnIII A1-D, and one-way ANOVA with Fisher's LSD test for FnIII A1-D. Statistical significance is displayed as * $p < 0.05$, ** $p < 0.01$, **** $p < 0.0001$ and non-significant (ns).

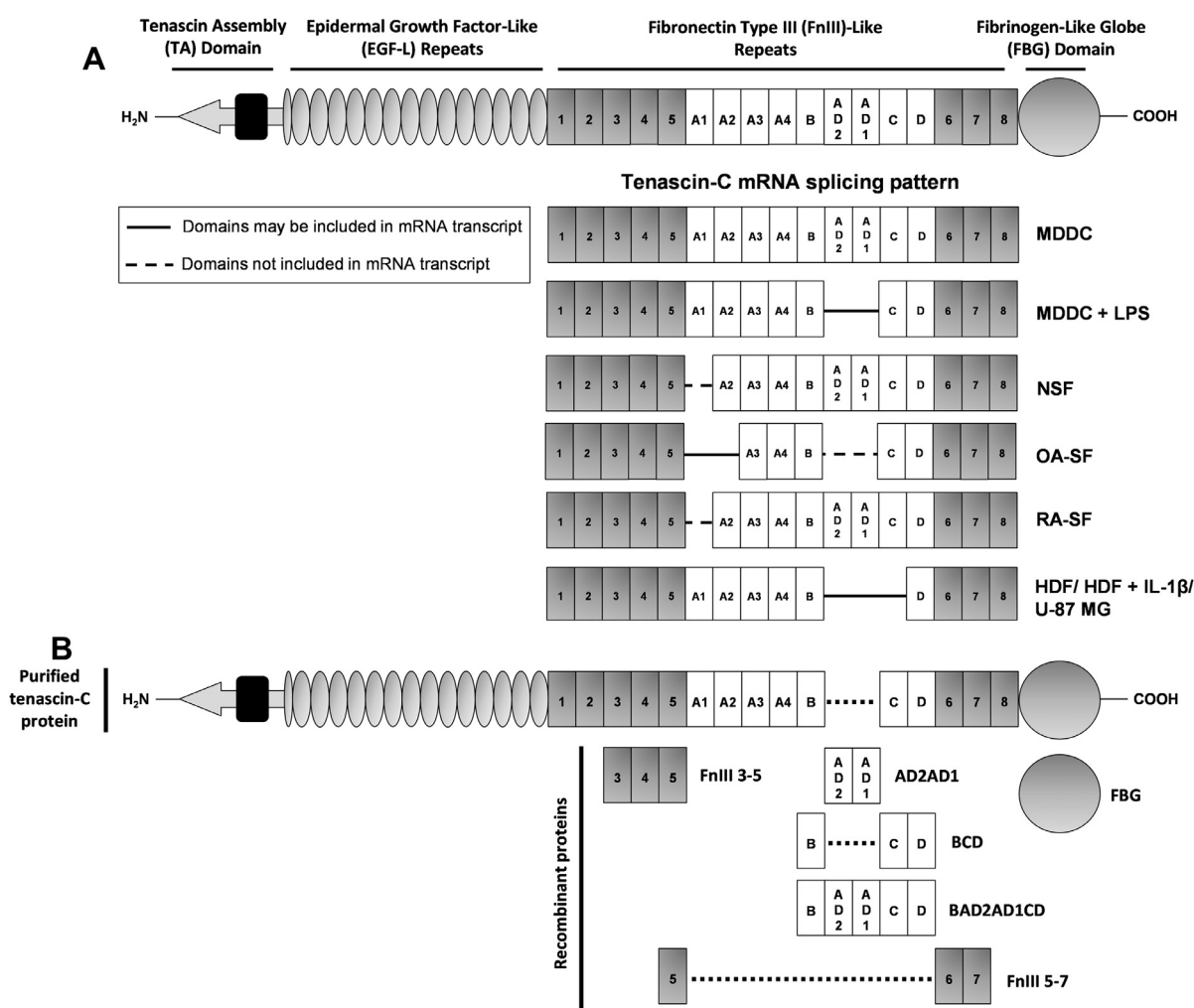


Fig. 4. Strategy for functional analysis of tenascin-C isoforms identified in immune cells and synovial fibroblasts. Schematic representation of full length tenascin-C containing the N-terminal tenascin assembly domain (TA), followed by 14.5 epidermal growth factor-like repeats (EGF-L), and up to 17 fibronectin type III-like repeats (FnIII), of which 8 are constitutively expressed (1–8; grey) and 9 are alternatively spliced (A1, A2, A3, A4, B, AD2, AD1, C and D; white), capped with a fibrinogen-like globe domain (FBG) (A; top panel). Alternative splicing patterns of tenascin-C mRNA transcripts expressed in resting MDDCs, and following stimulation with 10 ng/ml LPS, and in NSF, OA-SFs and RA-SFs (A; bottom panels). Proteins available, or synthesized, for subsequent functional studies include recombinant full-length tenascin-C protein lacking only the FnIII AD2/AD1 cassette, and recombinant proteins comprising FnIII domains 3–5, 5–7, AD2AD1, BCD, BAD2AD1CD and FBG. Boxes separated by a dotted line represent contiguity (B).

domains. Proteins were cloned, expressed and purified as described in [27] (**Supplementary figure S2A-D**); we also purified full-length tenascin-C containing all FnIII except AD2AD1, the constitutively expressed FnIII domains 3–5 and 5–7, and the C-terminal fibrinogen-like globe (FBG) for use as positive and negative controls [27] (**Fig. 4B**).

Alternatively spliced FnIII domains differentially support stromal and immune cell adhesion

Tenascin-C has long been known to modulate fibroblast adhesion, inducing loss of firm

attachment and disassembly of focal contacts [28, 29]. The location of these anti-adhesive properties somewhere within the alternatively spliced FnIII domains [30–33], prompted us to examine whether removal of domains AD2AD1 might impact cell adhesion. Consistent with published data, full length tenascin-C promoted little fibroblast adhesion [34, 35], whilst HDF adhered with low EC₅₀ and high B_{max} to both fibronectin [34] and to the cryptic β1 integrin binding site containing FnIII 3–5 [36]. All of the alternatively spliced FnIII domains supported greater HDF adhesion than tenascin-C, with significantly higher B_{max} levels

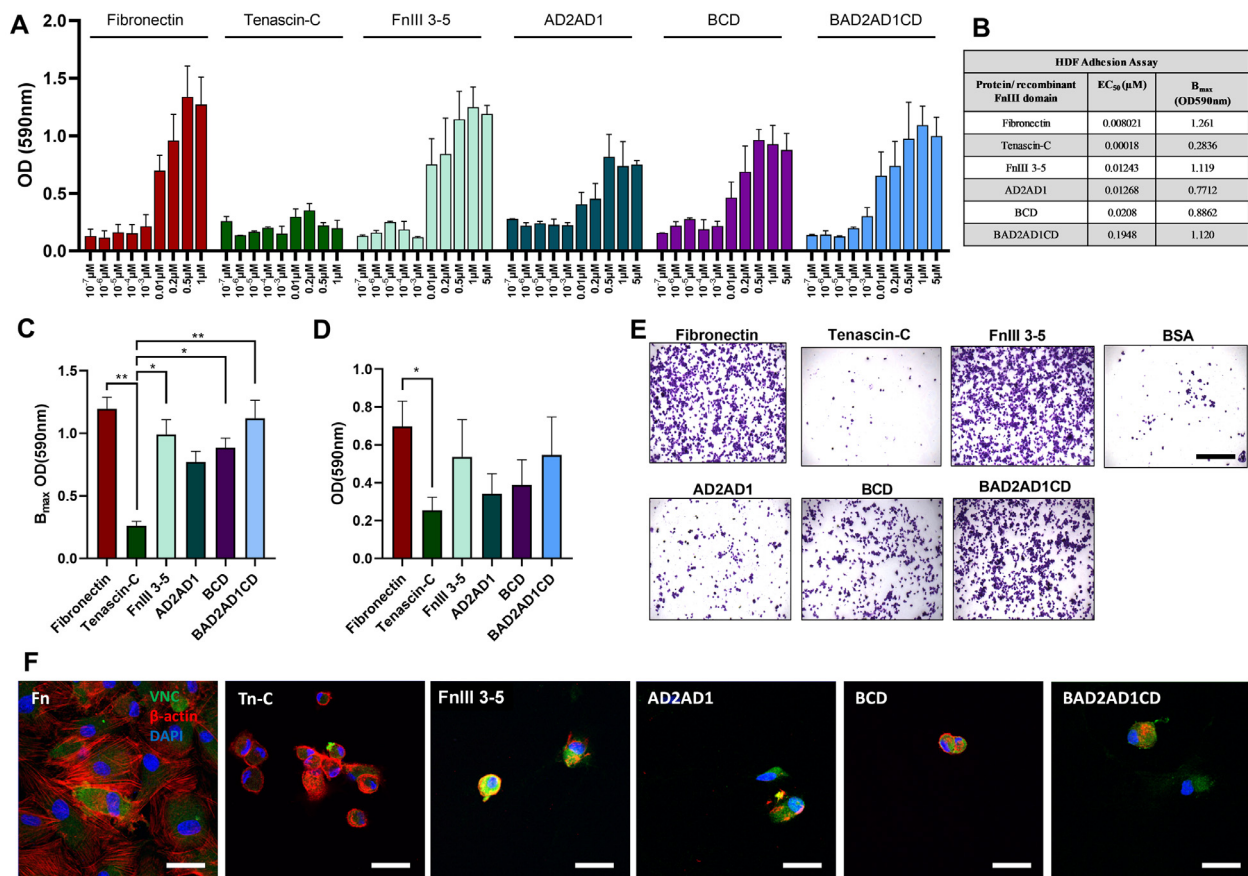


Fig. 5. Alternatively spliced FnIII domains support greater fibroblast adhesion than full-length tenascin-C. HDF adhesion to 96-well plates coated with the stated concentrations of fibronectin, tenascin-C, FnIII 3–5, AD2AD1, BCD and BAD2AD1CD, was assessed by staining with crystal violet. Data are shown as mean + SEM, from 6 separate experiments ($n = 6$) with the BSA blank value subtracted (A). EC₅₀ and B_{max} values were calculated and B_{max} values were plotted to show statistically significant differences (B, C) ($n = 3$). Data from cells plated on 0.01 μM of each substrate is shown (D) ($n = 6$), along with representative images (E) ($n = 4$). Scale bar = 100 μm. Data are shown as mean + SEM. One-way ANOVA was performed for (A), and one-way ANOVA with Turkey's multiple comparison tests for (C–D). Statistical significance is displayed as $*p < 0.05$, $**p < 0.01$. Immunofluorescence staining of β-actin (red), vinculin (Vnc) (green) and DAPI (blue) in HDFs cultured on glass coverslips coated with 0.01 μM fibronectin (Fn), tenascin-C (Tn-C), FnIII 3–5, AD2AD1, BCD, or BAD2AD1CD. Representative images from 3 separate experiments are shown. Scale bar = 20 μm (F). (For interpretation of the references to color in this figure legend, the reader is referred to the web version of this article.)

recorded for BCD and BAD2AD1CD. However, adhesion to BAD2AD1CD was greater than to AD2AD1 and BCD, with B_{max} values comparable to fibronectin and FnIII 3–5, although with higher EC₅₀ (Fig. 5A–E). Confocal immunofluorescence of HDFs cultured on glass slides coated with different substrates, and stained for vinculin and actin, revealed that HDFs spread well on fibronectin, but remained rounded on all other substrates. Only HDFs plated on FnIII 3–5 and BCD exhibited colocalization of actin and vinculin at the cell periphery, which was observed to a greater degree in cells on FnIII 3–5. HDFs adherent to tenascin-C, AD2AD1 and BAD2AD1CD exhibited diffuse vinculin staining throughout the cytosol,

while actin was present in distinct foci that did not overlap (Fig. 5F). These data indicate that, like FnIII 3–5, domains BAD2AD1CD, BCD and AD2AD1 support HDF adhesion better than full length tenascin-C, and that whilst HDFs do not spread on any tenascin-C derived substrate, adhesion to FnIII 3–5 and BCD promotes coherent actin and vinculin co-localization.

The ability of tenascin-C to support myeloid cell adhesion has yet not been reported. Surprisingly, and in contrast to HDF, dendritic cells adhered well to both fibronectin and full-length tenascin-C, and less well to FnIII 3–5. The alternatively spliced domains supported less dendritic cell adhesion than equimolar concentrations of full-length tenascin-C,

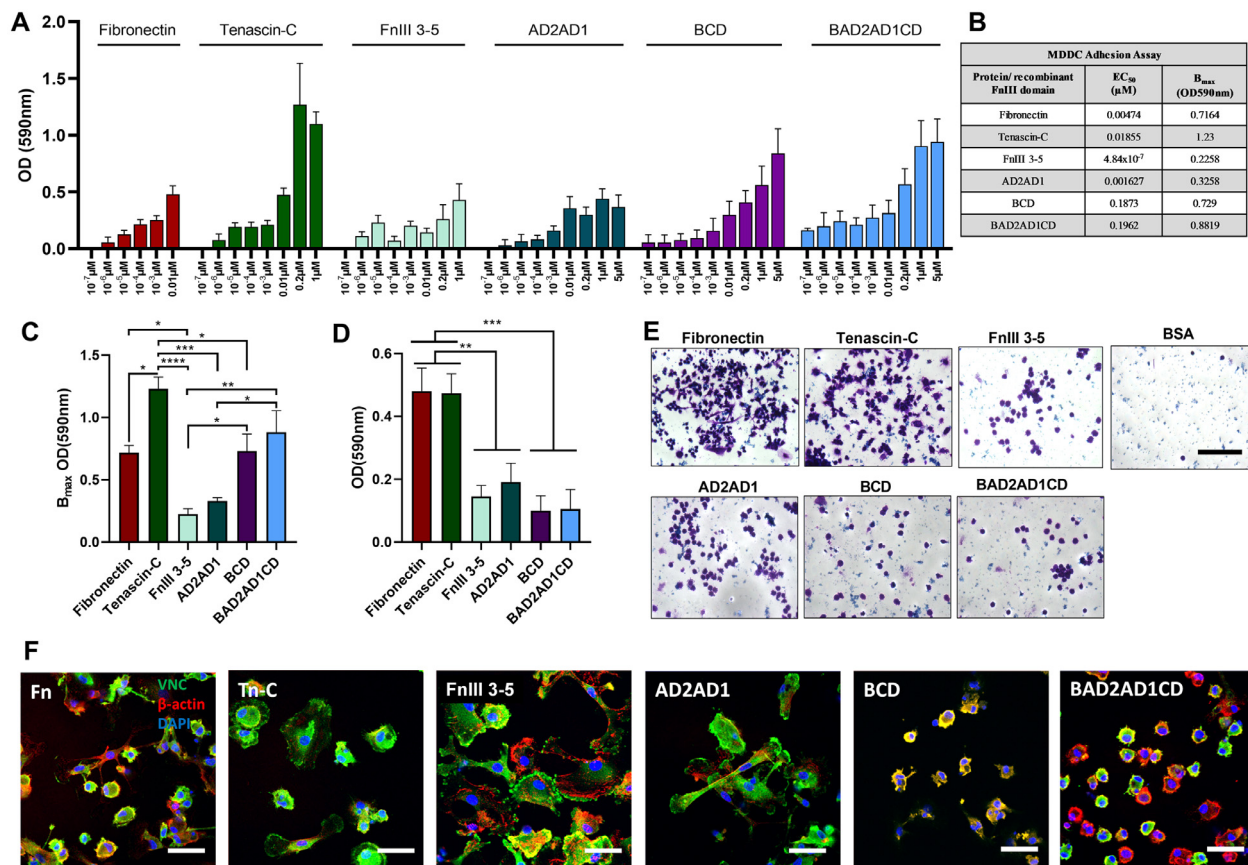


Fig. 6. Alternatively spliced FnIII domains exert different morphological effects on dendritic cells. MDDC adhesion to 96-well plates coated with the stated concentrations of fibronectin, tenascin-C, FnIII 3–5, AD2AD1, BCD and BAD2AD1CD, was assessed by staining with crystal violet. Data are shown as mean + SEM, from 3 separate experiments ($n = 3$) with the BSA blank value subtracted (A). EC₅₀ and B_{max} values were calculated and displayed in the table, while B_{max} values were plotted to show statistically significant differences (B, C) ($n = 3$). Data from cells plated on 0.01 μM of each substrate is shown (D) ($n = 3$), along with representative images (E) ($n = 3$). Scale bar = 100 μm. Data are shown as mean + SEM. One-way ANOVA was performed for (A), and one-way ANOVA with Turkey's multiple comparison tests for (C–D). Statistical significance is displayed as * $p < 0.05$, ** $p < 0.01$, *** $p < 0.001$, and **** $p < 0.0001$. Immunofluorescence staining of β-actin (red), vinculin (Vnc) (green) and DAPI (blue) in MDDCs cultured on glass coverslips coated with 0.01 μM fibronectin (Fn), tenascin-C (Tn-C), FnIII 3–5, AD2AD1, BCD, or BAD2AD1CD. Representative images from 3 separate experiments are shown. Scale bar = 20 μm (F). (For interpretation of the references to color in this figure legend, the reader is referred to the web version of this article.)

and there were no significant differences in the levels of adhesion between equimolar concentrations of FnIII 3–5, AD2AD1, BCD and BAD2AD1CD. However, there were significant differences in the maximal levels of MDDC adhesion to FnIII proteins; BCD and BAD2AD1CD supported significantly higher B_{max} values than FnIII 3–5, and BAD2AD1CD supported a significantly greater B_{max} than FnIII AD2AD1 (Fig. 6A–E). Confocal immunofluorescence of dendritic cells exhibited varied phenotypes. On tenascin-C dendritic cells were larger and more spread than on fibronectin; here, vinculin staining was concentrated at the centre of the cell and clustered in a ring around the edges, where it co-localised with actin. Cells plated on FnIII 3–5 and AD2AD1 also were larger and more spread

than on fibronectin, with short actin fibrils and vinculin clusters localising in lamellipodia at the cell edges. Dendritic cells cultured on BAD2AD1CD or BCD were morphologically similar, and were smaller and more rounded than those on fibronectin, tenascin-C, FnIII 3–5 and AD2AD1; containing many short processes. However, whilst most cells on BAD2AD1CD stained positive for either actin or vinculin, with a minority of cells staining positive for both, every cell plated on BCD showed strong co-localization of actin and vinculin at the edges of the cells (Fig. 6F).

Together these data suggest that full-length tenascin-C supports dendritic cell adhesion better than its isolated constituent domains, but that the opposite is true for HDFs, where multiple cryptic

binding sites exist including in FnIII 3–5 and in the alternatively spliced domains AD2AD1, BCD and BAD2AD1CD. Moreover, whilst different domains supported similar levels of cell adhesion, they invoked very different cell morphologies, and cellular organization of the actin cytoskeleton, indicating that whilst splicing of tenascin-C during inflammation may not quantitatively affect HDF adhesion, it may effect dendritic cell adhesion and might promote different cell behaviours upon each substrate.

BCD, but not BAD2AD1CD, promotes myeloid cell chemotaxis and cytokine release

The morphology of dendritic cells adherent to tenascin-C and different FnIII domains prompted us to examine if these proteins differently affect cell migration. We used a transwell assay to assess both passive migration, as a model of non-specific cell roaming, and directed migration of cells towards a chemotactic stimulus. We calculated the migration index as a measure of the mean number of migrated cells in response to stimulus divided by the number of passively migrated cells [37]. In line with previous data, dendritic cells demonstrated high levels of chemotaxis towards fetal bovine serum (FBS) when plated on fibronectin and bovine serum albumin (BSA) coated transwell inserts, and little passive migration in the absence of chemotactic stimulus [38]. In contrast, dendritic cells plated on transwells coated with tenascin-C, FnIII 3–5, AD2AD1 and BAD2AD1CD predominantly exhibited passive migration, and little directed chemotaxis. Conversely, cells plated on BCD exhibited high levels of chemotaxis towards FBS, and low levels of passive migration, resulting in a significantly higher migration index than observed on tenascin-C and all other FnIII, comparable to fibronectin (Fig. 7A–C). Together these data show that the alternatively spliced BCD domain is unique amongst the FnIII domains examined in supporting directed chemotaxis, whilst other regions of tenascin-C instead support dendritic cell roaming.

Finally, we examined the impact of alternative splicing in the BAD2AD1CD cassette on immune cell activation. Tenascin-C induces cytokine and chemokine expression in various cell types (reviewed in [20]). We identified that the FBG domain of the molecule induces IL-6 and TNF α secretion in human macrophages in a toll-like receptor 4 (TLR4) dependent manner, but found that recombinant proteins comprising three contiguous FnIII domains from the constitutively expressed region of tenascin-C including FnIII 1–3, FnIII 3–5, FnIII 5–7, and FnIII 6–8 did not induce any cytokine expression [27]. Here, we stimulated macrophages with LPS, FBG and FnIII 5–7 as positive and negative controls respectively. Both LPS and FBG

induced significant IL-6 release, whilst FnIII 5–7 had no effect, as expected. In the same experiments AD2AD1 and BAD2AD1CD were also unable to stimulate IL-6 release, whilst BCD did (Fig. 7D, E). Denaturation of BCD by boiling, or digestion with proteinase K, ablated the ability of this domain to induce cytokine release, whilst preincubation with polymyxin-B had no effect on protein activity, but did ablate LPS activity (Fig. 7F). Pre-incubation of cells with TAK242, a small molecule TLR4 antagonist, before treatment with BCD ablated cytokine synthesis (Fig. 7G). These data suggest that FnIII BCD can stimulate macrophage cytokine secretion in a TLR4 dependent manner but that AD2AD1 and BAD2AD1CD do not.

Discussion

Tenascin-C can exist as more than 500 different isoforms. However, despite growing evidence of the importance of alternatively spliced variants of this matrix molecule in embryogenesis and cancer, surprisingly little is known about tenascin-C expression during inflammation and in inflammatory disease. To begin to understand more about how post-transcriptional processing of tenascin-C dictates its function in immunity we undertook a systematic analysis of tenascin-C expression, localization and splicing in a panel of primary human immune cells before and after activation with inflammatory stimuli, and in healthy and diseased fibroblasts. This work identified lineage- and activation status-specific biosynthesis of tenascin-C, as well as common splicing events associated with immune and stromal cell activation. Our data reveal a hitherto unknown regulatory role for the alternatively spliced FnIII domains AD2AD1, that exert control over the impact that this matrix molecule has on cell adhesion and migration, and its ability to trigger innate immune signalling.

Firstly, we found unexpectedly different modes of tenascin-C biosynthesis in stromal and immune cells. Tenascin-C mRNA was abundantly and constitutively expressed in dermal fibroblasts, but detected at low levels in resting myeloid cells, where expression was transiently switched on following activation with inflammatory stimuli, then rapidly switched off. Tenascin-C protein was assembled into a fibrillar matrix at the surface of dermal fibroblasts, but not in activated myeloid cells, where it was exclusively trafficked through the cell and secreted. These data reveal cell-lineage-specific control over tenascin-C transcription, and highlight that this matrix molecule can exist as distinct molecular forms. It may be that immune cells lack receptors necessary to retain tenascin-C at the cell surface, or that they produce tenascin-C variants lacking binding sites for cell receptors or matrix components that are required for fibril formation. The

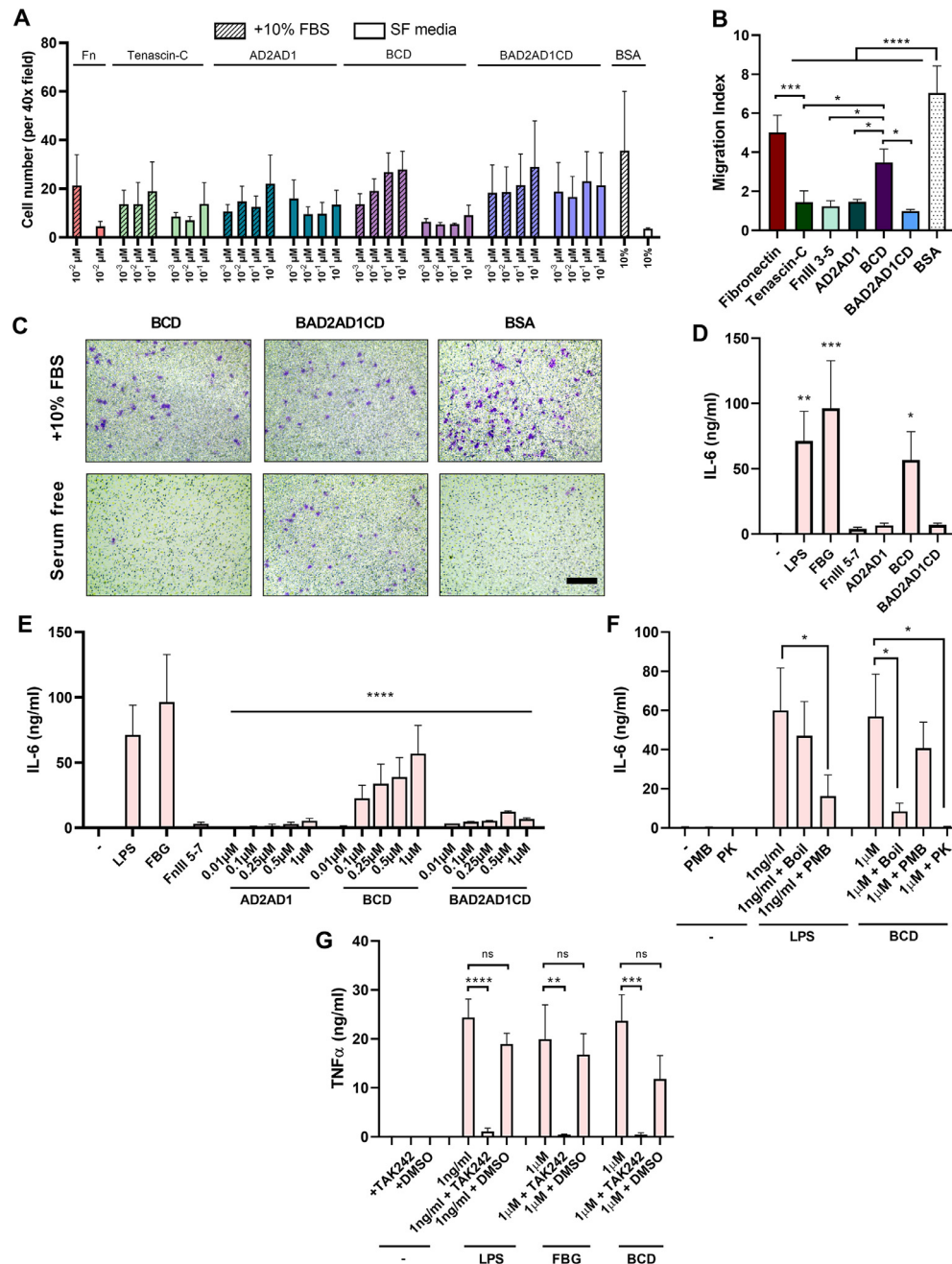


Fig. 7. Removal of domains AD2AD1 promotes immune cell chemotaxis and cytokine release. (A–C) Passive MDDC migration (clear bars) or MDDC chemotaxis towards FBS (hatched bars) was quantified using 24-well transwell inserts coated with the stated concentrations of fibronectin (Fn), tenascin-C, FnIII 3–5, AD2AD1, BCD, BAD2AD1CD, and BSA (10%), following removal of cells from the upper chamber and counting crystal violet stained cells on the underside of the membrane. The number of cells from 3 representative 40x fields per well were counted (A) ($n = 3$). The migration index was calculated by dividing the number of passively migrated cells into serum free medium by the number of cells migrated into medium containing 10% FBS for each substrate at 0.01 μ M (B). Representative images of fixed and stained membranes show MDDCs that migrated to the underside of the membranes coated with 0.01 μ M substrate (C). Scale bar = 100 μ m. (D–G) ($n = 4$) M-CSF macrophages from 4 independent donors were left unstimulated (-), or were stimulated with 1 ng/ml LPS, or with 1 μ M FBG, FnIII 5–7, AD2AD1, BCD or BAD2AD1CD for 24 h, before cytokine release was quantified by ELISA (D). Macrophages were stimulated with 1 ng/ml LPS, with 1 μ M FBG or FnIII 5–7, or with the stated doses of AD2AD1, BCD or BAD2AD1CD for 24 h (E). LPS and BCD were boiled, or treated with polymyxin B (PMB) or proteinase K for 30 min before cell stimulation (F). LPS, FBG and BCD were treated for 6 h with TAK242 or DMSO before cell stimulation (G). Data are shown as mean + SEM. One-way ANOVA with Fisher's LSD multiple comparisons were performed for (B,D,F,G), and two-way ANOVA with Turkey's multiple comparisons for (E). * $p < 0.05$, ** $p < 0.01$, *** $p < 0.001$, **** $p < 0.0001$ and non-significant (ns).

possibility also arises that these distinct forms exert different effects on cell behaviour, for example by modulating the mechanical properties of the tissue microenvironment, or by controlling receptor availability, affinity and/or avidity. This architectural flexibility may also enable tenascin-C to exert effects across multiple sub-tissular ranges, for example providing autocrine/local cues to cells surrounded by fibrillar matrix scaffolds, or as long-range, soluble cues capable of mediating wider/systemic paracrine effects.

Despite differences in tenascin-C biosynthesis we also observed commonalities in alternative splicing within the FnIII domains BAD2AD1CD in immune cells and synovial fibroblasts. Resting myeloid cells expressed all nine of the alternatively spliced FnIII domains at comparable levels, and synovial fibroblasts from healthy joints, or from the joints of people with OA, all except FnIII A1. In contrast, isoforms lacking domains AD1 and AD2 predominated in activated myeloid cells and synovial fibroblasts from the joints of people with RA. Identification of domains A1, A2, A3, A4, B, AD2, AD1, C and D in quiescent myeloid cells and non-inflamed synovial fibroblasts indicates that expression of the alternatively spliced domains of tenascin-C is more widespread than development and cancer, and that these domains are not exclusively associated with pathology in adult tissues. These data also highlight a novel immune-regulatory role for domains AD2AD1. Insertion of AD2AD1 within domains BCD created a FnIII domain organization that supported stromal cell adhesion, but prevented dendritic cell chemotaxis and TLR4-dependent macrophage cytokine synthesis; activities that were enabled upon removal of AD2AD1.

Little is known about domains AD1 and AD2. Only seven alternatively spliced FnIII domains were originally identified in tenascin-C. Additional domains (AD) 1 and AD2, were subsequently detected in cancer cells and in the developing chick embryo [39-41]. AD1 and AD2 are expressed by many human tumor cell lines including glioma, melanoma and sarcoma [39-44]. Both are also elevated in invasive breast cancer, with levels of either correlating with metastatic risk, and levels of AD1 with tamoxifen resistance in women younger than 40 years old. However, their expression is not tumor specific; low levels of both domains are observed in the duct myoepithelium of healthy breast [44, 45] and in the chick embryo AD1 expression largely mirrors tenascin-C localization at sites of tissue modelling, whilst AD2 is limited to regions of epithelial-mesenchymal interaction [40, 46]. Overexpression of domains BAD1D in breast cancer cell lines enhanced invasion and growth compared to variants lacking AD1 [45, 47], whilst AD2AD1C modulated chick myoblast adhesion, inhibiting binding to fibronectin [31], and promoting greater adhesion than variants containing no alternatively spliced FnIII domains, although cells

were irregularly shaped and lacked traditional focal adhesions on this substrate [28, 48, 49]. Together these data, and our results examining fibroblast and dendritic cell adhesion to BAD2AD1CD, indicate that expression of tenascin-C variants including AD1 and AD2 provides an environment conducive to tissue remodelling by permitting changes in motility, adhesion and cell shape. However, AD1 and AD2 are orphan domains with no binding partners identified to date, so it remains unclear how these effects are mediated. One possibility is that AD2AD1 modulates access to, or the affinity of, the $\alpha 7 \beta 1$ integrin binding site in FnIII D [18], although other, unknown, receptors for B, C or D may also play a role.

This is the first report linking AD2AD1 and inflammation, raising the question of how these domains control immune signalling. Structurally related, pro-inflammatory type III domains in fibronectin are also subject to post-transcriptional regulation, but here the inclusion of the alternatively spliced EDA domain, upregulated during tissue injury, confers TLR4 activating capabilities [50], rather than exclusion of inhibitory domains in tenascin-C that liberates inflammatory activity within BCD that is prohibited in BAD2AD1CD. These data imply a model in which the active epitope in BCD may comprise a region spanning domains FnIII B and C, which would be disrupted by the presence of AD2AD1. Indeed, the TLR4 binding site within the FBG domain of tenascin-C is not a linear epitope, but created by three distinct, non-contiguous sites [51]. Moreover, a cryptic TLR4 activation site is exposed in unfolded variants of the constitutively expressed FnIII 1 domain of fibronectin [52, 53], suggesting that proteolytic or mechanical remodelling of matrix molecule domain structure can control pro-inflammatory activity. Alternatively AD1 and AD2 might not act by precluding receptor ligation, but instead independently activate pathways that counteract TLR4-mediated signalling driven by domains BCD. For example, negative regulation of LPS-induced TLR4 activation is mediated by integrin signalling [54], whilst annexin II, a cell surface phospholipid-binding protein which binds somewhere within the 9 alternatively spliced domains of tenascin-C [55], downregulates cell surface TLR4 signalling by facilitating receptor translocation to the endosome [56]. Other alternatively spliced FnIII domains from tenascin-C are also linked to inflammation; A1 and A2 prevent anti-CD3/fibronectin mediated T-cell activation, by inhibiting T-cell receptor complex internalisation [57], A1, A2 and D inhibit T-cell transmigration and proliferation in vitro [57, 58], and a coding single nucleotide polymorphism in D associates with adult asthma [59, 60]. However, no further insight exists into any domain specific actions, and much more remains to be uncovered about tenascin-C splicing in immunity.

One key consideration in examining specific regions of large multidomain proteins such as

tenascin-C, is that individual domains, or linked modules of domains, are known to sometimes function differently in isolation than in the context of the full-length protein. In this way proteolytic degradation of large molecules creates 'matrikines'; smaller fragments that possess cryptic capabilities not present in the intact molecule [61]. Whilst we have demonstrated the ability of AD2AD1 to regulate the immune action of domains BCD within the context of the protein BAD2AD1CD, going forward it will be important to understand how immune activation via BCD, and control of this immune activation via AD2AD1, manifests in the context of full-length tenascin-C, or whether this cassette of domains exerts a cryptic function, liberated for example by cleavage at sites within the alternatively spliced FNIII repeats at sites of inflammation and tissue damage.

The recombinant proteins used in this study were generated in *E. coli* expression systems, as such they lack any mammalian post-translational modifications. However, the alternatively spliced domains of tenascin-C do contain putative sites for modification by glycosylation; within domains B, AD2, AD1, C and D, there are 8 and 6 putative *N*- and *O*-linked glycosylation sites respectively [13]. Whilst there are no data indicating these specific domains are modified *in situ* in human tissue; in mice the HNK-1 carbohydrate epitope is detected on FNIII C where it promotes neural stem cell proliferation and hippocampal neurite outgrowth [62, 63]. Another study shows that a glycosylated 220 kDa tenascin-C isoform plays a role in mediating neuronal cell adhesion [64]; but this is an area of tenascin-C biology that is not yet well explored. As such it will be important to keep in mind how post-translational modification of tenascin-C splice variants may add a further level of functional complexity to isoform biology [65].

Details around how tenascin-C splicing is controlled are beginning to emerge. Culture of healthy fibroblasts at neutral pH results in expression of small isoforms lacking domains FNIII A1-D [66-68], whilst culture in basic pH, or culture of malignantly transformed fibroblasts which maintain basic intracellular pH, results in predominant expression of large isoforms [67]. The RNA binding protein Sam68 drives preferential expression of large tenascin-C isoforms in neural stem cells [69], whilst splicing factor SRSF6 drives large isoform expression that is associated with keratinocyte hyperplasia *in vivo* [70]. Of relevance here, growth factors and cytokines not only up-regulate tenascin-C expression, but also modulate its post-transcriptional processing. For example, IL-4 induces long and short isoforms equally in keratinocytes, whilst TNF α preferentially induces short transcripts and IFN γ favors long transcripts [24]. TGF β -1 induces preferential expression of small tenascin-C isoforms lacking FNIII A1-D in endometrial adenocarcinoma and NIH-3T3 cells [71-73], whilst FGF-1 and -2 induce large variants in rat brain and NIH-3T3

fibroblasts [73-75]. These data illustrate how soluble mediators elevated at sites of inflammation could control FNIII domain composition, to trigger or resolve immune cell migration and activation.

Finally, elevated tenascin-C expression has been widely reported across many inflammatory diseases [20], including the autoimmune condition RA. Expression accumulates in inflamed synovia [23], where it is made by both fibroblasts and immune cells [23]; levels are also elevated in the circulation of people with RA [76]. Our data indicate that a switch in tenascin-C variants expressed by healthy synovial fibroblasts and resting myeloid cells, which contain the restraining domains AD2AD1, to variants lacking AD2AD1 in activated synovial fibroblasts and myeloid cells, could impact disease pathogenesis by promoting immune cell infiltration and cytokine synthesis, and inhibiting fibroblast adhesion, facilitating migration and invasion, all processes apparent in the RA joint (Fig. 8). Together these data uncover how the structural modularity of tenascin-C can be exploited to control its activity; designed to prevent unnecessary inflammation in healthy tissues, but to facilitate immune cell infiltration and activation when required, this study sheds light on how immunity triggered by endogenous danger signals can be controlled at the post-transcriptional level, and how this may go awry in autoimmune disease.

Experimental procedures

Cell isolation, culture and activation

Primary human monocytes and lymphocytes were isolated from plateletpheresis blood residues (North London Transfusion Centre), by ficoll gradient and counterflow centrifugation (Beckman GEL) [23]. Monocytes were plated at 1×10^6 cells/ml in 20 ml of RPMI-1640 with 5% fetal bovine serum (FBS; Gibco) and 1% Penicillin-Streptomycin (PS; Lonza), and differentiated into macrophages by culturing for 5 days with either 100 ng/ml colony-stimulating factor (M-CSF) or 50 ng/ml granulocyte-macrophage colony stimulating factor (GM-CSF). Monocytes were differentiated into monocyte derived dendritic cells (MDDC) by culturing for 7 days with 50 ng/ml GM-CSF and 10 ng/ml IL-4 [23]. T-cell subsets were purified using the CD3+ pan T-cell isolation kit (130-096-535), CD4+ T-cell isolation kit (130-091-155) or CD8+ microbeads (130-045-201) with LS columns (310-042-401) and a MidiMACSTM separator (Miltenyi), following manufacturer's instructions. Neutrophils were isolated by Andreea Ciuntu in the laboratory of Dr Lynne Prince (University of Sheffield), from human peripheral blood as described in [77]. All immune cells were cultured in RPMI-1640 containing 5% FBS and 1% PS. The U87-MG

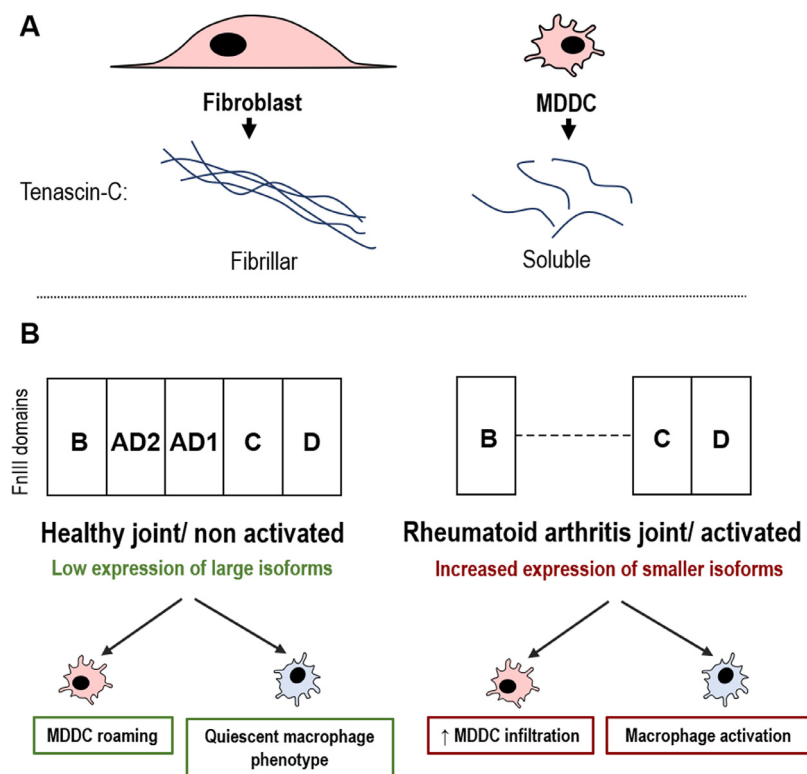


Fig. 8. A novel immuno-regulatory role for AD2AD1? The cartoon images summarize the fibrillar and soluble nature of tenascin-C synthesized by fibroblasts and dendritic cells (MDDC)(A), and proposes a model for the contribution of alternative splicing of tenascin-C in the balance and dysregulation of the immune axis in healthy and inflamed joints, wherein different isoforms detected in normal synovial fibroblasts compared to rheumatoid arthritis synovial fibroblasts, and in resting and activated MDDC, create immunologically inert or active variants of this endogenous innate immune trigger (B).

glioblastoma cell line and primary human dermal fibroblasts were purchased from ATCC. NSFs were obtained from people without arthritis, undergoing limb amputation or joint biopsy. OA-SFs and RA-SFs were obtained from waste synovial tissue from joint replacement surgeries. In all cases tissue was obtained after signed, informed consent and subject to local ethics approval [27, 78]. Fibroblasts and glioma cells were cultured in Dulbecco's Modified Eagles Medium (DMEM; Lonza) supplemented with 10% FBS and 1% PS and were passaged with trypsin-EDTA (Lonza) upon reaching 80% confluence. Fibroblasts were used in experiments between passages 2–6. For activation studies, monocytes, GM-CSF macrophages, M-CSF macrophages, MDDCs, neutrophils, CD4⁺ T-cells, CD8⁺ T-cells and HDFs were stimulated using well-established protocols for each cell type [86–92], and are detailed in **supplementary table S1**.

Quantification of tenascin-C mRNA by standard curve qPCR

Total RNA was extracted from cells using the RNeasy Mini Kit (Qiagen) and reverse transcribed

into cDNA using the AffinityScript cDNA synthesis kit and oligo(dT) primers (Agilent). RNA and DNA concentration and purity was assessed using the NanoDrop-1000 spectrophotometer (Thermo Scientific). The abundance of tenascin-C mRNA (*TNC*) was quantified by standard curve qPCR using, using a ViiA7 thermocycler (Applied Biosystems). 10 μ l qPCR reactions were prepared in triplicate, comprising of 2 μ l FAM-conjugated TaqManTM primers/probes, 5 μ l TaqManTM Universal PCR Master Mix (ThermoFisher Scientific), and 3 μ l of cDNA diluted 1:4 in H₂O. A fully sequenced IM.A.G.E cDNA clone for *TNC* (Source BioScience) was used to generate the standard curve; plasmid purity and concentration was assessed by NanoDrop-1000, and 10-fold serial dilutions prepared ranging from 10⁸ to 10⁻¹ copies/ μ l. No template controls were included in each assay. Standard curve data analysis was performed using ViiA7 software, to quantify the absolute copies mRNA/ μ l in cDNA samples.

For activated cells, 2-standard curve qPCR was performed using expression of an endogenous control gene in parallel with *TNC* expression. The stability of a number of different housekeeping

genes, was determined in each cell type, upon activation, over time, with the least variably expressed selected as a control. Relative quantifications were calculated by normalizing absolute copies/cell values for the gene of interest, against those for the endogenous control gene, or were calculated using the delta-delta Ct ($\Delta\Delta Ct$) qPCR method. A full list of FAM-conjugated TaqManTM primers (ThermoFisher Scientific), and the corresponding I.M.A.G.E cDNA clone plasmids (Source Bioscience) used for analysis of tenascin-C and housekeeping gene expression are listed in **supplementary table S2**.

Analysis of tenascin-C protein by ELISA and western blotting

Cell culture supernatant was aspirated from resting and activated cells alongside samples of unconditioned culture media, which served as a media blank. Adherent cells were lysed in-well and suspension cells were pelleted by centrifugation at 1500 rpm for 5 min, prior to lysis with low-SDS RIPA buffer, at a ratio of 200 μ l per 5×10^5 cells, for 25 min on ice. Total protein concentration in cell lysate was quantified with BCA protein assay kit (Pierce). Optical density at 562 nm (OD_{562nm}) was measured using the FluoStar Omega plate reader, and the sample protein concentration was calculated from a BSA standard curve. Tenascin-C levels in cell lysate and supernatant samples were analysed using the Tenascin-C Large (FnIII B) ELISA Assay Kit (#27767, IBL); in this assay the capture antibody 4C8MS binds to the FnIII B domain, while the secondary HRP-labelled antibody 4F10TT binds to the constitutive EGF-like domains. For SDS-PAGE, protein samples were denatured in SDS-loading buffer at 95°C for 5 min, and sonicated using a Bioruptor water bath (Diagenode) for 5 min. Cell lysate and supernatant were resolved on 5% SDS-PAGE tris-glycine gels alongside 6 μ l 250 kDa protein-plus molecular weight marker (ThermoFisher Scientific). Separated proteins were electrotransferred using the Trans-Blot Turbo Transfer System, to Trans-Blot Turbo mini nitrocellulose membranes (BioRad), using the 180 V high molecular weight program. Membranes were blocked with 5% BSA in PBS, 0.05% Tween-20 for 1 h at room temperature, then probed with mouse anti-human tenascin-C mAb (mAb1908; Millipore; 1:1000) that recognizes the N-terminal domain of the protein; followed by staining with anti-mouse IgG-HRP (BioRad; 1:20,000) secondary antibody and visualization using the enhanced chemo-luminescence (ECL) Plus kit (Amersham). Membranes of cell lysate samples were stripped with Restore Western blot stripping buffer (ThermoFisher Scientific), prior to re-staining with mouse anti-human vinculin mAb (SPM227; Novus; 1:1000), or mouse anti-human actin mAb (AB6276; Abcam; 1:1000).

Confocal immunofluorescence microscopy of tenascin-C

MDDCs, HDFs, NSFs, OA-SFs and RA-SFs were seeded onto 18 mm glass coverslips (VWR), in a 12-well tissue culture plate in 1 ml of medium. MDDCs and HDFs were stimulated as described above, and N-, OA- and RA-SF were cultured without stimulation for 24 h. Cells were fixed with 4% paraformaldehyde for 20 min at room temperature, then permeabilised, where stated, with 0.2% triton X-100 for 10 min. Cells were rinsed with PBS and blocked with 10% goat serum, before staining with mouse-anti human tenascin-C (BC-24; Sigma-Aldrich; 1:100) and rabbit anti-human fibronectin (F3648; Sigma-Aldrich; 1:200) antibodies at 4 °C for 16 h. Cells were then washed and stained with 1:250 4',6-diamidino-2-phenylindole (DAPI) (ThermoFisher Scientific), goat anti-mouse 488 nm (1:1000) and anti-rabbit 568 nm secondary (1:1000) antibodies for 1 h at room temperature. Coverslips were mounted on glass slides using ProLong anti-fade Gold (ThermoFisher Scientific). Slides were visualized with the Olympus FV1200 IX83 Confocal System using 60x objective lens and 2x zoom; and Z-axis stacked composite images were prepared from $n = 45$, 0.4 μ m step scans. Isotype control experiments (Mouse IgG1 isotype control; P30.6.2.8.1; ThermoFisher Scientific) and no-primary antibody control experiments were performed to assess non-specific staining.

Quantification of alternatively spliced FnIII domains by standard curve qPCR

Primers were designed to anneal within exon sequences corresponding to *TNC* FnIII A1, A2, A3, A4, B, AD2, AD1, C, D and 7–8, and to control genes *GAPDH*, *RPLP0*, *HPRT1*, *GNB2L1* and *YWHAZ* (**supplementary table S3/ supplementary table S4**); and were used to quantify the abundance of each alternatively spliced domain of tenascin-C as described in [26]. Briefly, target mRNAs were quantified in duplicate, with wells containing neat cDNA (MDDC, GM-CSF macrophage, M-CSF macrophage), or 1:10 diluted cDNA (U-87 MG, HDF, NSF, OA-SF and RA-SF). Standard curves were generated using tenascin-C plasmid pBS KS II hTNC+AD2+AD1 (gifted by Gertraud Orend; INSERM Strasbourg, FR) or I.M.A.G.E fully sequenced cDNA clone plasmids (**supplementary table S2**) at 10-fold serial dilutions from 10^6 to 10^{-1} copies/ μ l. Reverse transcriptase negative controls, and no-template controls were included for all PCR reactions.

Expression and purification of recombinant proteins

Purified recombinant tenascin-C [79], fibronectin purified from human plasma [80] and FnIII 3–5 [79]

were provided by Dr Wing To for use in this study. N-terminally His-tagged recombinant proteins corresponding to tenascin-C domains AD2AD1, BCD and BAD2AD1CD were cloned, expressed and purified as previously described for constitutively expressed tenascin-C domains [27]. Briefly, domain boundaries were identified using UniProt and corresponding DNA sequences amplified by high fidelity Phusion PCR using primers specified in **supplementary table S5**. cDNA clones pBS KS II hTNC+AD2+AD1 (tenascin-C with AD2 and AD1) or pBS KS II hTNC (tenascin-C without domains AD2 or AD1) (gifted by Gertraud Orend; INSERM Strasbourg, FR) were used as templates. Proteins were expressed in *E. coli* BL21 (DE3) pLysS cells and purified using two sequential rounds of Ni²⁺ chromatography (Bio-Rad). Each column was washed with 100 column volumes of 0.1% Triton-X114 (Sigma-Aldrich, laboratory grade 9036–19–5, lot no. 072k0049) to remove LPS, followed by washing with 100 column volumes of binding buffer, before protein elution using 150 mM imidazole. Proteins were characterized by silver staining and anti-His-Western blot. Protein secondary structure was analysed using the J-815 Circular Dichroism Spectrometer (Jasco), in 50 mM Tris, 150 mM NaCl pH8.0 buffer; with an optical path length of 10 mm. The CD spectrum was measured in the ‘far UV’ spectral region (190–250 nm) in samples at 20°C or following boiling for 10 min. Five repeated sample measurements were taken, from which CD spectra of sample buffer alone was subtracted, and mean averages were plotted and analysed using Spectra Manager™ software. CD spectra were deconvolved using Dichro-web [81], CONTINLL algorithm [82, 83] against reference set 7 [84, 85], with output in mean residue ellipticity. Endotoxin levels were measured using the Endpoint Chromogenic LAL Assay (Lonza). Each stock solution of protein was assayed using a protein concentration equivalent to the highest concentration added in cellular assays; typical preps contained between 1 and 8 pg/ml, and any prep exceeding 10pg/ml was discarded.

Cell adhesion assays

96-well tissue culture plates were coated with 50 µl of tenascin-C, fibronectin or tenascin-C domains diluted in PBS to concentrations from 1 µM to 10^{−9} µM, at 4 °C for 16 h. Wells were washed twice with PBS then blocked with 10% BSA in PBS for 2 h at room temperature before addition of 100 µl of serum free media. HDFs and MDDCs were plated at 4 × 10⁵ cells/ml and 1 × 10⁶ cells/ml in 100 µl of serum free DMEM and RPMI-1640 media respectively and left to adhere at 37 °C for 60 min. Plates were washed gently with PBS, and cells were fixed

in 4% PFA for 20 min at room temperature before staining with 0.1% crystal violet solution for 60 min. Excess dye was removed with 2-(N-morpholino)-ethanesulfonic acid (MES) buffer, and cells imaged with the Nikon Eclipse Ts2R light microscope using 20x and 40x objective lenses. Cells were then lysed in 100 µl 10% SDS for 5 min. Solubilised dye was measured at OD_{590nm} using the FluoStar Omega plate reader.

Immunofluorescence microscopy of cell morphology and cytoskeleton organization

Lab-Tek 8-well chamber slides (ThermoFisher Scientific) were coated with 150 µl of 0.01 µM fibronectin, tenascin-C, or tenascin-C domains at 4 °C for 16 h before washing with PBS and blocking in 10% BSA/PBS for 2 h at room temperature. HDFs and MDDCs were plated at 4 × 10⁵ cells/ml and 1 × 10⁶ cells/ml in 100 µl of serum free DMEM and RPMI-1640 media respectively and left to adhere at 37 °C for 60 min. Cells were stained with mouse anti-human vinculin primary antibody (SPM227; Abcam; 1:400) at 4 °C for 16 h. Secondary antibody staining was performed using goat anti-mouse AlexaFluor® 488 nm (1:1000), AlexaFluor® 568 nm phalloidin (1:400), and DAPI (1:250), while shielded from light for 2 h at room temperature. Alongside all experiments no-primary antibody controls were performed. Coverslips were mounted as described for confocal immunofluorescence staining, and confocal immunofluorescence images were obtained using the Olympus FV1200 confocal microscope, with a 60x objective lens and 2x optical zoom.

Transwell cell migration assays

Transwell inserts with 5 µm pores (Sigma-Aldrich) were coated with 10^{−2} µM fibronectin, 10^{−1}, 10^{−2}, 10^{−3} µM tenascin-C, or 1, 10^{−1}, 10^{−2}, 10^{−3} µM FnIII 5–7, AD2AD1, BCD, BAD2AD1CD or 10% BSA at 4°C for 16 h. Inserts were washed with PBS and blocked with 10% BSA/PBS for 1 h at room temperature before 600 µl serum free media RPMI-1640 with 1%, or 600 µl RPMI-1640 10% FBS 1% PS was added to the lower chamber. MDDCs at 1 × 10⁶ cells/ml in 100 µl serum free RPMI-1640 1% PS was added to the upper chamber and incubated for 3 h at 37°C. Media was then aspirated and cells removed from the upper chamber using a cotton bud. Migrated MDDCs on the underside of the Transwell membrane were fixed in 4% PFA for 20 min at room temperature, then stained with 0.1% crystal violet solution for 1 h at room temperature. Excess dye was removed with MES buffer, and membranes photographed in 3 locations using the Nikon Eclipse

Ts2R light microscope with 20x and 40x objective lens. Migrated cell counts were derived from the mean number of positively stained cells present in a 40x field, and the migration index (MI) was calculated by dividing the mean number of migrated cells in response to chemoattractant, by the mean number of passively migrated cells in the absence of chemoattractant; as described in [37].

Cytokine expression assays

M-CSF macrophages were plated at 5×10^5 cells/ml in 200 μ l RPMI-1640 5% FBS 1% P/S in a 96-well plate. Cells were rested for 16 h prior to stimulation with 1 ng/ml LPS, 1 μ M FBG, 1 μ M FnIII 5–7 or 1, 0.5, 0.25, 0.1 0.01 μ M AD2AD1, BCD or BAD2AD1CD. Stimuli were boiled at 95 °C for 30 min, treated with 1 U proteinase K (Sigma-Aldrich) for 1 h at 37 °C, or pre-incubated with 1 μ g/ml polymyxin-B (PMB) (Merck) for 30 min at 37 °C where indicated. Cells were pre-incubated with 3 μ M TAK242 (Merck) TLR4 inhibitor for 6 h at 37 °C prior to stimulation where stated. Supernatant was collected 24 h following stimulation. Cell viability was assessed by MTT assay and IL-6 and TNF α cytokine levels assayed by ELISA (BD Biosciences) as previously described in [27]. OD_{450nm} was recorded on FluoStar Omega plate reader.

EC₅₀ and B_{max}

EC₅₀ refers to the half maximal effective concentration, and B_{max} refers to the maximum specific binding of ligand observed in the assay. EC₅₀ and B_{max} values were calculated using non-linear regression software on GraphPad Prism 8.0, with the protein substrate concentration plotted on the X-axis, and OD_{590nm} from lysed cells plotted on the Y-axis. Curves were fit with non-linear regression (with Log₁₀ X-axis); EC₅₀ was calculated as the concentration of ligand at which half-maximal binding was observed, while B_{max} was calculated as the OD_{590nm} at which maximum specific binding was detected.

Statistical analysis

Data means, + SEM, + STDEV, and statistical analysis were calculated using GraphPad Prism 8.0 software. Multiple group means of more than 3 samples were subject to one-way analysis of variance by ANOVA with either Turkey's or Dunnett's multiple comparison tests, or Fisher's LSD multiple comparisons test where multiple comparisons stand alone to reduce false negative detection (Type II error), where appropriate. The analysis of variance of two independent variables were assessed by 2-way ANOVA with Sidak's multiple comparison corrections, or Fisher's LSD test when appropriate. Two-

tailed paired and un-paired t-tests were used for experiments involving only two groups where those samples came from identical or different populations respectively. *P* values less than 0.05 were considered significant.

Data availability

All relevant data are available from the authors.

Funding

This work was supported by PhD Prize Studentship from the Kennedy Trust for Rheumatology Research to SPG and a Versus Arthritis Senior Fellowship to KSM (20003).

Author contributions

KSM conceptualized the study and supervised the project. SPG and KSM designed the experiments. SPG validated the techniques used, acquired cell samples, generated recombinant proteins, performed the research, and analysed data. SPG and KSM interpreted the results. SPG and KSM wrote the manuscript. AS provided purified recombinant FBG protein and contributed to data interpretation. All authors read and approve the manuscript.

Declaration of Competing Interest

KSM is founder of, and consultant to, Nascent Ltd. All other authors have no declarations to make.

Acknowledgments

The authors would like to thank Lynne Prince and Andreea Ciuntu at the University of Sheffield for providing cDNA from activated human neutrophils.

Supplementary materials

Supplementary material associated with this article can be found, in the online version, at [doi:10.1016/j.matbio.2020.06.003](https://doi.org/10.1016/j.matbio.2020.06.003).

Received 29 April 2020;

Received in revised form 15 June 2020;

Accepted 21 June 2020

Available online 27 June 2020

Keywords:

Alternative splicing;
Extracellular matrix;
Tenascin-C;
Inflammation;
Rheumatoid arthritis

Abbreviations:

FBG, fibrinogen-like globe domain of tenascin-c; FnIII, fibronectin type III-like repeats; HDF, human dermal fibroblast; LPS, lipopolysaccharide; MDDC, monocyte derived dendritic cell; NSF, normal synovial fibroblast; OA-SF, osteoarthritis synovial fibroblasts; RA, rheumatoid arthritis; RA-SF, rheumatoid arthritis synovial fibroblast; TLR4, toll-like receptor 4; *TNC*, tenascin-C mRNA

References

- [1] M. Jain, S. Koren, K.H. Miga, J. Quick, A.C. Rand, T.A. Sasani, J.R. Tyson, A.D. Beggs, A.T. Dilthey, I.T. Fiddes, S. Malla, H. Marriott, T. Nieto, J. O'Grady, H.E. Olsen, B.S. Pedersen, A. Rhie, H. Richardson, A.R. Quinlan, T.P. Snutch, L. Tee, B. Paten, A.M. Phillippy, J.T. Simpson, N.J. Loman, M. Loose, Nanopore sequencing and assembly of a human genome with ultra-long reads, *Nat. Biotechnol.* 36 (4) (2018) 338–345.
- [2] <https://www.genome.gov/human-genome-project/results>.
- [3] L.M. Urbanski, N. Leclair, O. Anczukow, Alternative-splicing defects in cancer: splicing regulators and their downstream targets, guiding the way to novel cancer therapeutics, *Wiley Interdiscip. Rev. RNA* 9 (4) (2018) e1476.
- [4] G. Biamonti, M. Catillo, D. Pignataro, A. Montecucco, C. Ghigna, The alternative splicing side of cancer, *Semin. Cell Dev. Biol.* 32 (2014) 30–36.
- [5] E. Lara-Pezzi, J. Gomez-Salinerio, A. Gatto, P. Garcia-Pavia, The alternative heart: impact of alternative splicing in heart disease, *J. Cardiovasc. Transl. Res.* 6 (6) (2013) 945–955.
- [6] C.K. Vuong, D.L. Black, S. Zheng, The neurogenetics of alternative splicing, *Nat. Rev. Neurosci.* 17 (5) (2016) 265–281.
- [7] B.K. Dredge, A.D. Polydorides, R.B. Darnell, The splice of life: alternative splicing and neurological disease, *Nat. Rev. Neurosci.* 2 (1) (2001) 43–50.
- [8] I. Evsyukova, J.A. Somarelli, S.G. Gregory, M.A. Garcia-Blanco, Alternative splicing in multiple sclerosis and other autoimmune diseases, *RNA Biol.* 7 (4) (2010) 462–473.
- [9] K.W. Lynch, Consequences of regulated pre-mRNA splicing in the immune system, *Nat. Rev. Immunol.* 4 (12) (2004) 931–940.
- [10] M. Goedert, Tau gene mutations and their effects, *Mov. Disord.* 12 (2005) S45–S52.
- [11] M. Hong, V. Zhukareva, V. Vogelsberg-Ragaglia, Z. Wszolek, L. Reed, B.I. Miller, D.H. Geschwind, T.D. Bird, D. McKeel, A. Goate, J.C. Morris, K.C. Wilhelmsen, G.D. Schellenberg, J.Q. Trojanowski, V.M. Lee, Mutation-specific functional impairments in distinct tau isoforms of hereditary FTDP-17, *Science* 282 (5395) (1998) 1914–1917.
- [12] Y. Shao, W. Chong, X. Liu, Y. Xu, H. Zhang, Q. Xu, Z. Guo, Y. Zhao, M. Zhang, Y. Ma, F. Gu, Alternative splicing-derived intersectin1-L and intersectin1-S exert opposite function in glioma progression, *Cell Death Dis.* 10 (6) (2019) 431.
- [13] S.P. Giblin, K.S. Midwood, Tenascin-C: form versus function, *Cell Adh. Migr.* 9 (1–2) (2015) 48–82.
- [14] P. Richter, M. Tost, M. Franz, A. Altendorf-Hofmann, K. Junker, L. Borsi, D. Neri, H. Kosmehl, H. Wunderlich, A. Berndt, B and C domain containing tenascin-C: urinary markers for invasiveness of urothelial carcinoma of the urinary bladder? *J. Cancer Res. Clin. Oncol.* 135 (10) (2009) 1351–1358.
- [15] T. Gecks, K. Junker, M. Franz, P. Richter, M. Walther, A. Voigt, D. Neri, H. Kosmehl, H. Wunderlich, M. Kiehntopf, A. Berndt, B domain containing Tenascin-C: a new urine marker for surveillance of patients with urothelial carcinoma of the urinary bladder? *Clin. Chim. Acta* 412 (21–22) (2011) 1931–1936.
- [16] G.S. Orend, F. Schwenzer, A. Midwood, *The Extracellular Matrix and Cancer: Regulation of Tumor Cell Biology by Tenascin-C*. KS. iConcept Press Ltd., USA, 2014.
- [17] D. Neri, Antibody-cytokine fusions: versatile products for the modulation of anticancer immunity, *Cancer Immunol. Res.* 7 (3) (2019) 348–354.
- [18] M.L. Mercado, A. Nur-e-Kamal, H.Y. Liu, S.R. Gross, R. Movahed, S. Meiners, Neurite outgrowth by the alternatively spliced region of human tenascin-C is mediated by neuronal alpha7beta1 integrin, *J. Neurosci.: Off. J. Soc. Neurosci.* 24 (1) (2004) 238–247.
- [19] A. Siri, V. Knauper, N. Veirana, F. Caocci, G. Murphy, L. Zardi, Different susceptibility of small and large human tenascin-C isoforms to degradation by matrix metalloproteinases, *J. Biol. Chem.* 270 (15) (1995) 8650–8654.
- [20] A.M. Marzeda, K.S. Midwood, Internal Affairs, Tenascin-C as a clinically relevant, endogenous driver of innate immunity, *J. Histochem. Cytochem.: Off. J. Histochem. Soc.* 66 (4) (2018) 289–304.
- [21] R.V. Iozzo, M.A. Gubbiotti, Extracellular matrix: the driving force of mammalian diseases, *Matrix Biol.: J. Int. Soc. Matrix Biol.* 71–72 (2018) 1–9.
- [22] S.S. McCachren, V.A. Lightner, Expression of human tenascin in synovitis and its regulation by interleukin-1, *Arthr. Rheum.* 35 (10) (1992) 1185–1196.
- [23] F.G. Goh, A.M. Piccinini, T. Krausgruber, I.A. Udaloova, K.S. Midwood, Transcriptional regulation of the endogenous danger signal tenascin-C: a novel autocrine loop in inflammation, *J. Immunol.* 184 (5) (2010) 2655–2662.
- [24] M.A. Latijnhouwers, G.J. de Jongh, M. Bergers, M.J. de Rooij, J. Schalkwijk, Expression of tenascin-C splice variants by human skin cells, *Arch. Dermatol. Res.* 292 (9) (2000) 446–454.
- [25] N. Brosicke, F.K. van Landeghem, B. Scheffler, A. Faissner, Tenascin-C is expressed by human glioma in vivo and shows a strong association with tumor blood vessels, *Cell Tissue Res.* 354 (2) (2013) 409–430.
- [26] S.P. Giblin, D. Murdamoohoo, C. Deligne, A. Schwenzer, G. Orend, K.S. Midwood, How to detect and purify tenascin-C, *Methods Cell Biol.* 143 (2018) 371–400.
- [27] K. Midwood, S. Sacre, A.M. Piccinini, J. Inglis, A. Trebaul, E. Chan, S. Drexler, N. Sofat, M. Kashiwagi, G. Orend, F. Brennan, B. Foxwell, Tenascin-C is an endogenous activator of Toll-like receptor 4 that is essential for maintaining inflammation in arthritic joint disease, *Nat. Med.* 15 (7) (2009) 774–780.
- [28] C.Y. Chung, J.E. Murphy-Ullrich, H.P. Erickson, Mitogenesis, cell migration, and loss of focal adhesions induced by tenascin-C interacting with its cell surface receptor, annexin II, *Mol. Biol. Cell* 7 (6) (1996) 883–892.

- [29] K.S. Midwood, J.E. Schwarzbauer, Tenascin-C modulates matrix contraction via focal adhesion kinase- and Rho-mediated signaling pathways, *Mol. Biol. Cell* 13 (10) (2002) 3601–3613.
- [30] J.E. Murphy-Ullrich, V.A. Lightner, I. Aukhil, Y.Z. Yan, H.P. Erickson, M. Hook, Focal adhesion integrity is downregulated by the alternatively spliced domain of human tenascin, *J. Cell Biol.* 115 (4) (1991) 1127–1136.
- [31] D. Fischer, R.P. Tucker, R. Chiquet-Ehrismann, J.C. Adams, Cell-adhesive responses to tenascin-C splice variants involve formation of fascin microspikes, *Mol. Biol. Cell* 8 (10) (1997) 2055–2075.
- [32] B. Gotz, A. Scholze, A. Clement, A. Joester, K. Schutte, F. Wigger, R. Frank, E. Spiess, P. Ekblom, A. Faissner, Tenascin-C contains distinct adhesive, anti-adhesive, and neurite outgrowth promoting sites for neurons, *J. Cell Biol.* 132 (4) (1996) 681–699.
- [33] M.A. Ghert, W.N. Qi, H.P. Erickson, J.A. Block, S.P. Scully, Tenascin-C splice variant adhesive/anti-adhesive effects on chondrosarcoma cell attachment to fibronectin, *Cell Struct. Funct.* 26 (3) (2001) 179–187.
- [34] R. Chiquet-Ehrismann, E.J. Mackie, C.A. Pearson, T. Sakakura, Tenascin: an extracellular matrix protein involved in tissue interactions during fetal development and oncogenesis, *Cell* 47 (1) (1986) 131–139.
- [35] W. Huang, R. Chiquet-Ehrismann, J.V. Moyano, A. Garcia-Pardo, G. Orend, Interference of tenascin-C with syndecan-4 binding to fibronectin blocks cell adhesion and stimulates tumor cell proliferation, *Cancer Res.* 61 (23) (2001) 8586–8594.
- [36] P. Joshi, C.Y. Chung, I. Aukhil, H.P. Erickson, Endothelial cells adhere to the RGD domain and the fibrinogen-like terminal knob of tenascin, *J. Cell. Sci.* 106 (Pt 1) (1993) 389–400.
- [37] N. Kramer, A. Walzl, C. Unger, M. Rosner, G. Krupitza, M. Hengstschlager, H. Dolznig, In vitro cell migration and invasion assays, *Mutat. Res.* 752 (1) (2013) 10–24.
- [38] B.G. Ricart, M.T. Yang, C.A. Hunter, C.S. Chen, D.A. Hammer, Measuring traction forces of motile dendritic cells on micropost arrays, *Biophys. J.* 101 (11) (2011) 2620–2628.
- [39] P. Sriram Rao, M.A. Bourdon, A novel tenascin type III repeat is part of a complex of tenascin mRNA alternative splices, *Nucl. Acids Res.* 21 (1) (1993) 163–168.
- [40] A.J. Mighell, J. Thompson, W.J. Hume, A.F. Markham, P.A. Robinson, Human tenascin-C, identification of a novel type III repeat in oral cancer and of novel splice variants in normal, malignant and reactive oral mucosae, *Int. J. Cancer* 72 (2) (1997) 236–240.
- [41] R.P. Tucker, J. Spring, S. Baumgartner, D. Martin, C. Hagios, P.M. Poss, R. Chiquet-Ehrismann, Novel tenascin variants with a distinctive pattern of expression in the avian embryo, *Development* 120 (3) (1994) 637–647.
- [42] S.C. Bell, J.H. Pringle, D.J. Taylor, T.M. Malak, Alternatively spliced tenascin-C mRNA isoforms in human fetal membranes, *Mol. Hum. Reprod.* 5 (11) (1999) 1066–1076.
- [43] A. Berndt, K. Anger, P. Richter, L. Borsi, S. Brack, M. Silacci, M. Franz, H. Wunderlich, M. Gajda, L. Zardi, D. Neri, H. Kosmehl, Differential expression of tenascin-C splicing domains in urothelial carcinomas of the urinary bladder, *J. Cancer Res. Clin. Oncol.* 132 (8) (2006) 537–546.
- [44] L.B. Derr, R. Chiquet-Ehrismann, R. Gandour-Edwards, J. Spence, R.P. Tucker, The expression of tenascin-C with the AD1 variable repeat in embryonic tissues, cell lines and tumors in various vertebrate species, *Differentiation* 62 (2) (1997) 71–82.
- [45] D.S. Guttery, R.A. Hancox, K.T. Mulligan, S. Hughes, S.M. Lambe, J.H. Pringle, R.A. Walker, J.L. Jones, J.A. Shaw, Association of invasion-promoting tenascin-C additional domains with breast cancers in young women, *Breast Cancer Res.: BCR* 12 (4) (2010) R57.
- [46] R.P. Tucker, S.E. McKay, The expression of tenascin by neural crest cells and glia, *Development* 112 (4) (1991) 1031–1039.
- [47] R.A. Hancox, M.D. Allen, D.L. Holliday, D.R. Edwards, C.J. Pennington, D.S. Guttery, J.A. Shaw, R.A. Walker, J.H. Pringle, J.L. Jones, Tumour-associated tenascin-C isoforms promote breast cancer cell invasion and growth by matrix metalloproteinase-dependent and independent mechanisms, *Breast Cancer Res.: BCR* 11 (2) (2009) R24.
- [48] J.C. Adams, J. Lawler, Cell-type specific adhesive interactions of skeletal myoblasts with thrombospondin-1, *Mol. Biol. Cell* 5 (4) (1994) 423–437.
- [49] C.Y. Chung, H.P. Erickson, Cell surface annexin II is a high affinity receptor for the alternatively spliced segment of tenascin-C, *J. Cell Biol.* 126 (2) (1994) 539–548.
- [50] Y. Okamura, M. Watari, E.S. Jerud, D.W. Young, S.T. Ishizaka, J. Rose, J.C. Chow, J.F. Strauss 3rd, The extra domain A of fibronectin activates Toll-like receptor 4, *J. Biol. Chem.* 276 (13) (2001) 10229–10233.
- [51] L. Zuliani-Alvarez, A.M. Marzeda, C. Deligne, A. Schwenzer, F.E. McCann, B.D. Marsden, A.M. Piccinini, K.S. Midwood, Mapping tenascin-C interaction with toll-like receptor 4 reveals a new subset of endogenous inflammatory triggers, *Nat. Commun.* 8 (1) (2017) 1595.
- [52] R. You, M. Zheng, P.J. McKeown-Longo, The first type III repeat in fibronectin activates an inflammatory pathway in dermal fibroblasts, *J. Biol. Chem.* 285 (47) (2010) 36255–36259.
- [53] R. Kelsh, R. You, C. Horzempa, M. Zheng, P.J. McKeown-Longo, Regulation of the innate immune response by fibronectin: synergism between the III-1 and EDA domains, *PLoS One* 9 (7) (2014) e102974.
- [54] P.J. McKeown-Longo, P.J. Higgins, Integration of canonical and noncanonical pathways in TLR4 signaling: complex regulation of the wound repair program, *Adv. Wound Care (New Rochelle)* 6 (10) (2017) 320–329.
- [55] X.G. Gong, Y.F. Lv, X.Q. Li, F.G. Xu, Q.Y. Ma, Gemcitabine resistance induced by interaction between alternatively spliced segment of tenascin-C and annexin A2 in pancreatic cancer cells, *Biol. Pharm. Bull.* 33 (8) (2010) 1261–1267.
- [56] S. Zhang, M. Yu, Q. Guo, R. Li, G. Li, S. Tan, X. Li, Y. Wei, M. Wu, Annexin A2 binds to endosomes and negatively regulates TLR4-triggered inflammatory responses via the TRAM-TRIF pathway, *Sci. Rep.* 5 (2015) 15859.
- [57] M.D. Puente Navazo, D. Valmori, C. Ruegg, The alternatively spliced domain TnFnIII A1A2 of the extracellular matrix protein tenascin-C suppresses activation-induced T lymphocyte proliferation and cytokine production, *J. Immunol.* 167 (11) (2001) 6431–6440.
- [58] K. Parekh, S. Ramachandran, J. Cooper, D. Bigner, A. Patterson, T. Mohanakumar, Tenascin-C, over expressed in lung cancer down regulates effector functions of tumor infiltrating lymphocytes, *Lung Cancer* 47 (1) (2005) 17–29.
- [59] A. Matsuda, T. Hirota, M. Akahoshi, M. Shimizu, M. Tamari, A. Miyatake, A. Takahashi, K. Nakashima, N. Takahashi, K. Obara, N. Yuyama, S. Doi, Y. Kamogawa, T. Enomoto, K. Ohshima, T. Tsunoda, S. Miyatake, K. Fujita, M. Kusakabe, K. Izuhara, Y. Nakamura, J. Hopkin, T. Shirakawa, Coding SNP in tenascin-C Fn-III-D domain

- associates with adult asthma, *Hum. Mol. Genet.* 14 (19) (2005) 2779–2786.
- [60] D.N. O'Dwyer, S.J. Gurczynski, B.B. Moore, Pulmonary immunity and extracellular matrix interactions, *Matrix Biol.: J. Int. Soc. Matrix Biol.* 73 (2018) 122–134.
- [61] J.M. Wells, A. Gaggari, J.E. Blalock, MMP generated matrikines, *Matrix Biol.: J. Int. Soc. Matrix Biol.* 44–46 (2015) 122–129.
- [62] H. Yagi, M. Yanagisawa, Y. Suzuki, Y. Nakatani, T. Ariga, K. Kato, R.K. Yu, HNK-1 epitope-carrying tenascin-C spliced variant regulates the proliferation of mouse embryonic neural stem cells, *J. Biol. Chem.* 285 (48) (2010) 37293–37301.
- [63] A. Nakamura, J. Morise, K. Yabuno-Nakagawa, Y. Hashimoto, H. Takematsu, S. Oka, Site-specific HNK-1 epitope on alternatively spliced fibronectin type-III repeats in tenascin-C promotes neurite outgrowth of hippocampal neurons through contactin-1, *PLoS One* 14 (1) (2019) e0210193.
- [64] J. Kruse, G. Keilhauer, A. Faissner, R. Timpl, M. Schachner, The J1 glycoprotein—a novel nervous system cell adhesion molecule of the L2/HNK-1 family, *Nature* 316 (6024) (1985) 146–148.
- [65] R.D. Sanderson, S.K. Bandari, I. Vlodavsky, Proteases and glycosidases on the surface of exosomes: newly discovered mechanisms for extracellular remodeling, *Matr. Biol.: J. Int. Soc. Matrix Biol.* 75–76 (2019) 160–169.
- [66] D. Neri, C.T. Supuran, Interfering with pH regulation in tumours as a therapeutic strategy, *Nat. Rev. Drug Discov.* 10 (10) (2011) 767–777.
- [67] L. Borsi, G. Allemanni, B. Gaggero, L. Zardi, Extracellular pH controls pre-mRNA alternative splicing of tenascin-C in normal, but not in malignantly transformed, cells, *Int. J. Cancer* 66 (5) (1996) 632–635.
- [68] L. Borsi, E. Balza, B. Gaggero, G. Allemanni, L. Zardi, The alternative splicing pattern of the tenascin-C pre-mRNA is controlled by the extracellular pH, *J. Biol. Chem.* 270 (11) (1995) 6243–6245.
- [69] S. Moritz, S. Lehmann, A. Faissner, A. von Holst, An induction gene trap screen in neural stem cells reveals an instructive function of the niche and identifies the splicing regulator sam68 as a tenascin-C-regulated target gene, *Stem Cells* 26 (9) (2008) 2321–2331.
- [70] M.A. Jensen, J.E. Wilkinson, A.R. Krainer, Splicing factor SRSF6 promotes hyperplasia of sensitized skin, *Nat. Struct. Mol. Biol.* 21 (2) (2014) 189–197.
- [71] C.A. Pearson, D. Pearson, S. Shibahara, J. Hofsteenge, R. Chiquet-Ehrismann, Tenascin: cDNA cloning and induction by TGF-beta, *EMBO J.* 7 (10) (1988) 2977–2982.
- [72] J. Chimal-Monroy, L. Diaz de Leon, Expression of N-cadherin, N-CAM, fibronectin and tenascin is stimulated by TGF-beta1, beta2, beta3 and beta5 during the formation of precartilaginous condensations, *Int. J. Dev. Biol.* 43 (1) (1999) 59–67.
- [73] R.P. Tucker, R. Chiquet-Ehrismann, The regulation of tenascin expression by tissue microenvironments, *Biochim. Biophys. Acta* 1793 (5) (2009) 888–892.
- [74] R.P. Tucker, J.A. Hammarback, D.A. Jenrath, E.J. Mackie, Y. Xu, Tenascin expression in the mouse: in situ localization and induction in vitro by bFGF, *J. Cell. Sci.* 104 (Pt 1) (1993) 69–76.
- [75] S. Suzuki, A.J. Li, M. Ikemoto, T. Imamura, Expression of tenascin-C long isoforms is induced in the hypothalamus by FGF-1, *Neuroreport* 13 (8) (2002) 1041–1045.
- [76] T.H. Page, P.J. Charles, A.M. Piccinini, V. Nicolaidou, P.C. Taylor, K.S. Midwood, Raised circulating tenascin-C in rheumatoid arthritis, *Arthritis Res. Ther.* 14 (6) (2012) R260.
- [77] P.L. Parker LC, D.J. Buttle, I. Sabroe, The Generation of Highly Purified Primary Human Neutrophils and Assessment of Apoptosis in Response to Toll-Like Receptor Ligands, in: O.N.L. McCoy CE (Ed.), *Toll-Like Receptors: Methods and Protocols*, Humana Press, Totowa, NJ, USA, 2009, pp. 191–204.
- [78] F.M. Brennan, D. Chantry, A. Jackson, R. Maini, M. Feldmann, Inhibitory effect of TNF alpha antibodies on synovial cell interleukin-1 production in rheumatoid arthritis, *Lancet* 2 (8657) (1989) 244–247.
- [79] W.S. To, K.S. Midwood, Identification of novel and distinct binding sites within tenascin-C for soluble and fibrillar fibronectin, *J. Biol. Chem.* 286 (17) (2011) 14881–14891.
- [80] E. Engvall, E. Ruoslahti, Binding of soluble form of fibroblast surface protein, fibronectin, to collagen, *Int. J. Cancer* 20 (1) (1977) 1–5.
- [81] L. Whitmore, B.A. Wallace, Protein secondary structure analyses from circular dichroism spectroscopy: methods and reference databases, *Biopolymers* 89 (5) (2008) 392–400.
- [82] S.W. Provencher, J. Glockner, Estimation of globular protein secondary structure from circular dichroism, *Biochemistry* 20 (1) (1981) 33–37.
- [83] I.H. van Stokkum, H.J. Spoelder, M. Bloemendal, R. van Grondelle, F.C. Groen, Estimation of protein secondary structure and error analysis from circular dichroism spectra, *Anal. Biochem.* 191 (1) (1990) 110–118.
- [84] N. Sreerama, S.Y. Venyaminov, R.W. Woody, Estimation of protein secondary structure from circular dichroism spectra: inclusion of denatured proteins with native proteins in the analysis, *Anal. Biochem.* 287 (2) (2000) 243–251.
- [85] N. Sreerama, R.W. Woody, Estimation of protein secondary structure from circular dichroism spectra: comparison of CONTIN, SELCON, and CDSSTR methods with an expanded reference set, *Anal. Biochem.* 287 (2) (2000) 252–260.
- [86] S.R. McColl, R. Paquin, C. Menard, A.D. Beaulieu, Human neutrophils produce high levels of the interleukin 1 receptor antagonist in response to granulocyte/macrophage colony-stimulating factor and tumor necrosis factor alpha, *J. Exp. Med.* 176 (2) (1992) 593–598.
- [87] M. Malyak, M.F. Smith Jr., A.A. Abel, W.P. Arend, Peripheral blood neutrophil production of interleukin-1 receptor antagonist and interleukin-1 beta, *J. Clin. Immunol.* 14 (1) (1994) 20–30.
- [88] A.M. Piccinini, K.S. Midwood, Endogenous control of immunity against infection: tenascin-C regulates TLR4-mediated inflammation via microRNA-155, *Cell Rep* 2 (4) (2012) 914–926.
- [89] F.O. Martinez, S. Gordon, The M1 and M2 paradigm of macrophage activation: time for reassessment, *F1000Prime Rep.* 6 (2014) 13.
- [90] A. Trickett, Y.L. Kwan, T cell stimulation and expansion using anti-CD3/CD28 beads, *J. Immunol. Methods* 275 (1–2) (2003) 251–255.
- [91] R.H. Bohmer, L.S. Trinkle, J.L. Staneck, Dose effects of LPS on neutrophils in a whole blood flow cytometric assay of phagocytosis and oxidative burst, *Cytometry* 13 (5) (1992) 525–531.
- [92] A.P. Rapoport, C.N. Abboud, J.F. DiPersio, Granulocyte-macrophage colony-stimulating factor (GM-CSF) and granulocyte colony-stimulating factor (G-CSF): receptor biology, signal transduction, and neutrophil activation, *Blood Rev.* 6 (1) (1992) 43–57.